J|A|C|S ARTICLES

Published on Web 11/11/2010

Fast Reactivity of a Cyclic Nitrone−Calix[4]pyrrole Conjugate with Superoxide Radical Anion: Theoretical and Experimental Studies†

Shang-U Kim,‡,§ Yangping Liu,§ Kevin M. Nash,‡ Jay L. Zweier,§ Antal Rockenbauer,|| and Frederick A. Villamena*,‡,§

Department of Pharmacology and Center for Biomedical EPR Spectroscopy and Imaging, Davis Heart and Lung Research Institute, College of Medicine, The Ohio State University, Columbus, Ohio 43210, United States, and Institute of Structural Chemistry, Chemical Research Center, H-1025 Budapest, Pusztaszeri 59, Hungary

Received June 14, 2010; E-mail: frederick.villamena@osumc.edu

Abstract: Nitrone spin traps have been employed as probes for the identification of transient radical species in chemical and biological systems using electron paramagnetic resonance (EPR) spectroscopy and have exhibited pharmacological activity against oxidative-stress-mediated diseases. Since superoxide radical anion ($O_2^{\bullet-}$) is a major precursor to most reactive oxygen species and calix[4]pyrroles have been shown to exhibit high affinity to anions, a cyclic nitrone conjugate of calix[4]pyrrole (CalixMPO) was designed, synthesized, and characterized. Computational studies at the PCM/B3LYP/6-31+G(d,p)//B3LYP/6-31G(d) level suggest a pendant-type linkage between the calix[4]pyrrole and the nitrone to be the most efficient design for spin trapping of $O_2^{\bullet-}$, giving exoergic reaction enthalpies ($\Delta H_{298K,aq}$) and free energies ($\Delta G_{298K,aq}$) of −16.9 and −2.1 kcal/mol, respectively. ^{1}H NMR study revealed solvent-dependent conformational changes in CalixMPO leading to changes in the electronic properties of the nitronyl group upon H-bonding with the pyrrole groups as also confirmed by calculations. CalixMPO spin trapping of $O_2^{\bullet-}$ exhibited robust EPR spectra. Kinetic analysis of $O_2^{\bullet-}$ adduct formation and decay in polar aprotic solvents using UV−vis stopped-flow and EPR methods gave a larger trapping rate constant for CalixMPO and a longer half-life for its $O_2^{\bullet-}$ adduct compared to the commonly used nitrones. The unusually high reactivity of CalixMPO with $O_2^{\bullet-}$ was rationalized to be due to the synergy between the α-effect and electrostatic effect by the calix[4]pyrrole moiety on $O_2^{\bullet-}$ and the nitrone, respectively. This work demonstrates for the first time the application of an anion receptor for the detection of one of the most important radical intermediates in biological and chemical systems (i.e., $O_2^{\bullet-}$).

1. Introduction

Superoxide radical anion ($O_2^{\bullet-}$) is produced from one-electron reduction of the triplet dioxygen molecule and is an important precursor to some of the highly oxidizing species that are known to exist in chemical and biological systems.[1] Superoxide can be generated through chemical, photochemical, and enzymatic means. For example, $O_2^{\bullet-}$ production has been observed via photolysis of water-soluble fullerene C_{60} or quinones.[2] Superoxide is enzymatically produced via stimulation of NADPH oxidases,[3] leakage from the mitochondrial electron transport chain complexes,[4] oxidation of hypoxanthine by xanthine oxidase,[5] or uncoupled nitric oxide synthase.[6] In biological systems, the unregulated production of $O_2^{\bullet-}$ can lead to the formation of highly oxidizing species, causing cellular dysfunction through loss of protein function, carbohydrate oxidation, DNA cleavage, and lipid peroxidation, and ultimately is responsible for the development of a variety of diseases such as cardiovascular and neurodegenerative diseases,[7] cancer,[8] inflammation,[9] acute stroke,[10] or ischemia−reperfusion injury.[11]

† Presented in part at the Gordon Conference Oxygen Radicals Meeting, Ventura, CA, Feb 7−12, 2010.

‡ Department of Pharmacology, The Ohio State University.

§ Davis Heart and Lung Research Institute, The Ohio State University.

|| Chemical Research Center, Budapest.

(1) Afanas'ev, I. B. *Superoxide Ion: Chemistry and Biological Implications*; CRC Press: Boca Raton, FL, 1989; Vol. 1. Afanas'ev, I. B. *Superoxide Ion: Chemistry and Biological Implications*; CRC Press: Boca Raton, FL, 1991; Vol. 2.

(2) Crisostomo, A. G.; Moreno, R. B.; Navaratnam, S.; Wilkinson, J. A.; Bisby, R. H. *Free Radical Res.* **2007**, *41*, 730–737. Garg, S.; Rose, A. L.; Waite, T. D. *Photochem. Photobiol.* **2007**, *83*, 904–913. Yamakoshi, Y.; Sueyoshi, S.; Fukuhara, K.; Miyata, N.; Masumizu, T.; Kohno, M. *J. Am. Chem. Soc.* **1998**, *120*, 12363–12364.

(3) Lambeth, J. D. *Nat. Rev. Immunol.* **2004**, *4*, 181–189.

(4) Chen, Y.-R.; Chen, C.-L.; Yeh, A.; Liu, X.; Zweier, J. L. *J. Biol. Chem.* **2006**, *281*, 13159–13168.

(5) Harrison, R. *Free Radical Biol. Med.* **2002**, *33*, 774–797.

(6) Xia, Y.; Dawson, V. L.; Dawson, T. M.; Synder, S. H.; Zweier, J. L. *Proc. Natl. Acad. Sci. U.S.A.* **1996**, *93*, 6770–6774.

(7) Sayre, L. M.; Perry, G.; Smith, M. A. *Chem. Res. Toxicol.* **2008**, *21*, 172–188. Tsutsui, H.; Kinugawa, S.; Matsushima, S. *Cardiovasc. Res.* **2009**, *81*, 449–456.

(8) Dreher, D.; Junod, A. F. *Eur. J. Cancer, Part A* **1996**, *32A*, 30–38.

(9) Petrone, W. F.; English, D. K.; Wong, K.; McCord, J. M. *Proc. Natl. Acad. Sci. U.S.A.* **1980**, *77*, 1159–1163.

(10) Alexandrova, M. L.; Bochev, P. G. *Free Radical Biol. Med.* **2005**, *39*, 297–316.

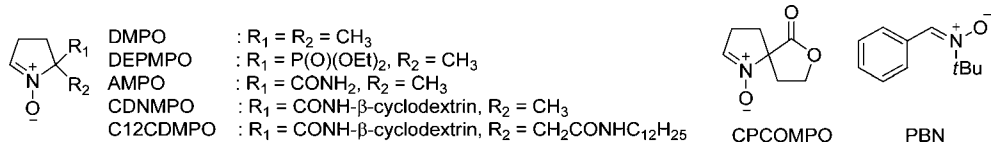

Figure 1. Structures of cyclic nitrone spin traps.

Electron paramagnetic resonance (EPR) spin trapping is a commonly used technique for radical detection which involves formation of radical adducts that exhibit a distinctive EPR spectrum. The direct or indirect observations of $O_2^{\bullet-}/HO_2^{\bullet}$ formation have been achieved by spin trapping using melanosomes,[12] mitochondria,[13] photosynthetic systems,[14] nitric oxide synthase (NOS),[6,15] endothelial cells,[16] human neutrophils,[17] and reperfused heart tissue.[18,19] Spin trapping has also found a wide range of applications in the fields of fuel cell research,[20] nanotechnology,[21] catalysis,[22] environmental remediation,[23] and photodynamic therapy.[24] In spite of the popularity of the cyclic nitrones, such as 5,5-dimethylpyrroline *N*-oxide (DMPO)[25] and 5-(diethoxyphosphoryl)-5-methylpyrroline *N*-oxide (DEPMPO),[26] these nitrones suffer from limitations such as slow reactivity with $O_2^{\bullet-}$ and poor $O_2^{\bullet-}$ adduct stability.[27]

Almost four decades ago[28] since the inception of nitrone spin traps as probes for radical detection, hundreds of new spin traps with improved properties have been synthesized,[29] but these spin traps still suffer from major limitations such as poor reactivity with $O_2^{\bullet-}$, a short adduct half-life, or nonspecificity to cellular compartments, or they exhibit a spectrum that cannot discern one radical adduct from another.[30] Our laboratory uses a computational approach for a rational design of spin traps with improved spin trapping properties.[31] By exploiting the nucleophilic nature of $O_2^{\bullet-}$ addition to nitrones, the electrophilicity of the nitronyl C (the site of $O_2^{\bullet-}$ addition) was increased through conjugation with an amide group at the C-5 position. Furthermore, initial H-bond interaction of the amide substituent with $O_2^{\bullet-}$ enhances its nucleophilicity to the nitrone via the α-effect.[32,33] Kinetic experimental studies showed that the amide-substituted nitrone (AMPO) exhibited a rate constant for $O_2^{\bullet-}$ trapping in DMF/H_2O of $k = 135\ M^{-1}\ s^{-1}$ compared to those of DMPO and DEPMPO of $k = 2.0$ and $0.7\ M^{-1}\ s^{-1}$, respectively (in H_2O, for AMPO, $k = 25\ M^{-1}\ s^{-1}$, for DMPO, $k = 2.0\ M^{-1}\ s^{-1}$, and, for DEPMPO, $k = 4.0\ M^{-1}\ s^{-1}$).[31] The H-bond donor rich β-cyclodextrin−nitrone conjugates CDNMPO and C12CDMPO, linked through an amide bond, gave k_2 values of 221 $M^{-1}\ s^{-1}$ (DMF/H_2O) and 72 $M^{-1}\ s^{-1}$ (H_2O), respectively.[34,35] The role of H-bond donors in increasing the $O_2^{\bullet-}$ nucleophilicity was further demonstrated by Winterbourn et al.[36] for tyrosyl hydroperoxide formation and was confirmed by our group to be due to the α-effect.[32] Improved $O_2^{\bullet-}$ adduct stability was also realized using CDNMPO through H-bond stabilization of the radical adduct, giving a maximum half-life in water of $t_{1/2} = 30$ min compared to those of DMPO and DEPMPO of $t_{1/2} = 1$ and 14 min, respectively (see Figure 1 for the structures).[34,35] However, the permethylated CD-

(11) Zweier, J. L.; Talukder, M. A. H. *Cardiovasc. Res.* **2006**, *70*, 181–190.
(12) Zareba, M.; Szewczyk, G.; Sarna, T.; Hong, L.; Simon, J. D.; Henry, M. M.; Burke, J. M. *Photochem. Photobiol.* **2006**, *82*, 1024–1029.
(13) Chen, Y.-R.; Chen, C.-L.; Yeh, A.; Liu, X.; Zweier, J. L. *J. Biol. Chem.* **2006**, *281*, 13159–13168. Dugan, L. L.; Sensi, S. L.; Canzoniero, L. M. T.; Handran, S. D.; Rothman, S. M.; Lin, T. S.; Goldberg, M. P.; Choi, D. W. *J. Neurosci.* **1995**, *15*, 6377–6388.
(14) Pospisil, P.; Arato, A.; Krieger-Liszkay, A.; Rutherford, A. W. *Biochemistry* **2004**, *43*, 6783–6792. Rahimipour, S.; Palivan, C.; Barbosa, F.; Bilkis, I.; Koch, Y.; Weiner, L.; Fridkin, M.; Mazur, Y.; Gescheidt, G. *J. Am. Chem. Soc.* **2003**, *125*, 1376–1384.
(15) Xia, Y.; Roman, L. J.; Masters, B. S. S.; Zweier, J. L. *J. Biol. Chem.* **1998**, *273*, 22635–22639. Xia, Y.; Tsai, A.-L.; Berka, V.; Zweier, J. L. *J. Biol. Chem.* **1998**, *273*, 25804–25808.
(16) Varadharaj, S.; Watkins, T.; Cardounel, A. J.; Garcia, J. G. N.; Zweier, J. L.; Kuppusamy, P.; Natarajan, V.; Parinandi, N. L. *Antioxid. Redox Signaling* **2005**, *7*, 287–300.
(17) Britigan, B. E.; Cohen, M. S.; Rosen, G. M. *J. Leukocyte Biol.* **1987**, *41*, 349–362.
(18) Wang, P.; Chen, H.; Qin, H.; Sankarapandi, S.; Becher, M. W.; Wong, P. C.; Zweier, J. L. *Proc. Natl. Acad. Sci. U.S.A.* **1998**, *95*, 4556–4560.
(19) Zweier, J. L.; Flaherty, J. T.; Weisfeldt, M. L. *Proc. Natl. Acad. Sci. U.S.A.* **1987**, *84*, 1404–1407. Zweier, J. L.; Kuppusamy, P.; Lutty, G. A. *Proc. Natl. Acad. Sci. U.S.A.* **1988**, *85*, 4046–4050. Zweier, J. L.; Kuppusamy, P.; Williams, R.; Rayburn, B. K.; Smith, D.; Weisfeldt, M. L.; Flaherty, J. T. *J. Biol. Chem.* **1989**, *264*, 18890–18895.
(20) Bosnjakovic, A.; Kadirov, M. K.; Schlick, S. *Res. Chem. Intermed.* **2007**, *33*, 677–687. Bosnjakovic, A.; Schlick, S. *J. Phys. Chem. B* **2006**, *110*, 10720–10728. Danilczuk, M.; Bosnjakovic, A.; Kadirov, M. K.; Schlick, S. *J. Power Sources* **2007**, *172*, 78–82.
(21) Babu, S.; Velez, A.; Wozniak, K.; Szydlowska, J.; Seal, S. *Chem. Phys. Lett.* **2007**, *442*, 405–408. Ionita, P.; Conte, M.; Gilbert, B. C.; Chechik, V. *Org. Biomol. Chem.* **2007**, *5*, 3504–3509. Kagan, V. E.; Tyurina, Y. Y.; Tyurin, V. A.; Konduru, N. V.; Potapovich, A. I.; Osipov, A. N.; Kisin, E. R.; Schwegler-Berry, D.; Mercer, R.; Castranova, V.; Shvedova, A. A. *Toxicol. Lett.* **2006**, *165*, 88–100.
(22) Fu, H.; Zhang, L.; Zhang, S.; Zhu, Y.; Zhao, J. *J. Phys. Chem. B* **2006**, *110*, 3061–3065.
(23) Xiao, G.; Wang, X.; Li, D.; Fu, X. *J. Photochem. Photobiol., A* **2008**, *193*, 213–221. Chang, Q.; He, H.; Zhao, J.; Yang, M.; Qu, J. *Environ. Sci. Technol.* **2008**, *42*, 1699–1704. Yu, J. C.; Ho, W.; Yu, J.; Yip, H.; Wong, P. K.; Zhao, J. *Environ. Sci. Technol.* **2005**, *39*, 1175–1179.
(24) Zeng, Z.; Zhou, J.; Zhang, Y.; Qiao, R.; Xia, S.; Chen, J.; Wang, X.; Zhang, B. *J. Phys. Chem. B* **2007**, *111*, 2688–2696. Rajendran, M.; Inbaraj, J. J.; Gandhidasan, R.; Murugesan, R. *J. Photochem. Photobiol., A* **2006**, *182*, 67–74. Mroz, P.; Pawlak, A.; Satti, M.; Lee, H.; Wharton, T.; Gali, H.; Sarna, T.; Hamblin, M. R. *Free Radical Biol. Med.* **2007**, *43*, 711–719.
(25) Finkelstein, E.; Rosen, G. M.; Rauckman, E. J. *J. Am. Chem. Soc.* **1980**, *102*, 4994–4999.
(26) Frejaville, C.; Karoui, H.; Tuccio, B.; le Moigne, F.; Culcasi, M.; Pietri, S.; Lauricella, R.; Tordo, P. *J. Chem. Soc., Chem. Commun.* **1994**, 1793–1794.
(27) Khan, N.; Wilmot, C. M.; Rosen, G. M.; Demidenko, E.; Sun, J.; Joseph, J.; O'Hara, J.; Kalyanaraman, B.; Swartz, H. M. *Free Radical Biol. Med.* **2003**, *34*, 1473–1481.
(28) Iwamura, M.; Inamoto, N. *Bull. Chem. Soc. Jpn.* **1967**, *40*, 703.
(29) Clement, J.-L.; Tordo, P. *Electron Paramagn. Reson.* **2007**, 29–49.
(30) Villamena, F. A.; Zweier, J. L. *Antioxid. Redox Signaling* **2004**, *6*, 619–629.
(31) Villamena, F. A.; Xia, S.; Merle, J. K.; Lauricella, R.; Tuccio, B.; Hadad, C. M.; Zweier, J. L. *J. Am. Chem. Soc.* **2007**, *129*, 8177–8191.
(32) Field, S. M.; Villamena, F. A. *Chem. Res. Toxicol.* **2008**, *21*, 1923–1932.
(33) Villamena, F. A.; Rockenbauer, A.; Gallucci, J.; Velayutham, M.; Hadad, C. M.; Zweier, J. L. *J. Org. Chem.* **2004**, *69*, 7994–8004.
(34) Han, Y.; Liu, Y.; Rockenbauer, A.; Zweier, J. L.; Durand, G.; Villamena, F. A. *J. Org. Chem.* **2009**, *74*, 5369–5380.
(35) Han, Y.; Tuccio, B.; Lauricella, R.; Villamena, F. A. *J. Org. Chem.* **2008**, *73*, 7108–7117.
(36) Winterbourn, C. C.; Parsons-Mair, H. N.; Gebicki, S.; Gebicki, J. M.; Davies, M. J. *Biochem. J.* **2004**, *381*, 241–248.

Table 1. Calculated Enthalpies (ΔH_{298K}) and Free Energies (ΔG_{298K}) (kcal/mol) for Complex Formation of *meso*-Octamethylcalix[4]pyrrole with the Selected Anions, Neutral Substrates, $O_2^{\bullet-}$, $HO_2^{\bullet}$, and $HO^{\bullet}$ in the Aqueous Phase and DMSO (in Parentheses) at the PCM/B3LYP/6-31+G(d,p)//B3LYP/6-31G(d) and PCM/B3LYP/6-311+G(d,p)//B3LYP/6-31G(d) Levels of Theory and Bond Length Ranges (Å) for the Pyrrole NH···X

	PCM/B3LYP/6-31+G(d,p)//B3LYP/6-31G(d)		PCM/B3LYP/6-311+G(d,p)//B3LYP/6-31G(d)		
X	ΔH_{298K}	ΔG_{298K}	ΔH_{298K}	ΔG_{298K}	NH···X
benzoate	5.4 (2.7)	19.3 (16.6)	5.8 (3.1)	19.7 (17.0)	1.81−1.89
Br^-	−9.3 (−12.9)	2.9 (−0.8)	7.5 (3.8)	19.6 (16.0)	2.43
Cl^-	3.4 (−0.6)	14.7 (10.7)	3.0 (−0.8)	14.4 (10.5)	2.34
CN^-	1.7 (3.2)	11.9 (13.5)	2.4 (−1.5)	12.6 (8.7)	2.05−2.07
$ONOO^-$	−5.5 (−9.4)	8.8 (5.0)	−6.3 (−10.1)	8.0 (4.2)	1.85−1.89
acetone	4.3 (0.4)	16.4 (12.4)	4.4 (0.5)	16.5 (12.5)	2.00
methanol	4.1 (0.3)	14.8 (11.0)	4.3 (0.4)	15.0 (11.2)	1.93
H_2O_2	3.15 (−1.2)	15.9 (11.6)	3.3 (−1.2)	16.0 (11.6)	2.07
$O_2^{\bullet-}$	−2.5 (−6.4)	9.2 (5.3)	−3.0 (−6.9)	8.7 (4.8)	1.84−1.87
$HO_2^{\bullet}$	−4.0 (−7.6)	9.3 (5.7)	−4.1 (−7.8)	9.2 (5.4)	1.76−1.80
$HO^{\bullet}$	−34.5 (−38.8)	−21.6 (−25.9)	−33.8 (−38.2)	−20.9 (−25.3)	1.74

DEPMPO gave a $t_{1/2}$ of 40 min,[37] indicating that factors other than intramolecular H-bonding can affect the adduct stability perhaps via van der Waals interaction.

As pioneered by Sessler and co-workers, a family of calixpyrroles have drawn significant attention in the field of molecular recognition for their convenient synthesis, as well as efficient and selective binding properties to anionic and neutral substrates.[38,39] Calix[4]pyrroles are macrocyclic molecules consisting of pyrrole rings linked via the 2- and 5-positions by sp^3-hybridized carbon atoms. Over the past few years, a large number of calixpyrrole derivatives have been synthesized such as the *meso*-alkyl-substituted,[40] halogenated,[41] *C*-rim-modified,[42] photoactive and chromophore-modified,[43] strapped,[44] ditopic,[45] expanded,[46] *N*-confused,[47] and polyfunctional[48] analogues exhibiting a variety of recognition properties. Due to the ubiquitousness of anions in many systems, calixpyrroles have been employed as ion-selective receptors[43] and anion-selective optical sensors.[49]

Because of the H-bond-donating properties of pyrrole NH, calix[4]pyrrole may exhibit selectivity toward $O_2^{\bullet-}$. We therefore hypothesized that calix[4]pyrrole conjugation with spin traps can offer improved spin trapping properties in terms of increased reactivity with $O_2^{\bullet-}$ and a longer $O_2^{\bullet-}$ adduct half-life. To the best of our knowledge, there has been no reported application of calix[4]pyrrole in spin trapping, and for the first time, this work describes the design, synthesis, and physicochemical characterization of a calix[4]pyrrole−nitrone conjugate exhibiting extraordinarily improved $O_2^{\bullet-}$ trapping properties and stability for the $O_2^{\bullet-}$ adduct formed, as compared to conventional spin traps.

2. Results and Discussion

2.1. Computational Studies. 2.1.1. Radical Binding to Calix[4]pyrrole. The thermodynamics of calix[4]pyrrole binding to various anions (e.g., benzoate, Br^-, Cl^-, and CN^-) and neutral substrates (e.g., acetone and MeOH) were calculated and compared to those of $O_2^{\bullet-}$ and its protonated form, $HO_2^{\bullet}$. Table 1 shows the enthalpies ($\Delta H_{298K,aq}$) and free energies ($\Delta G_{298K,aq}$) as well as bond distances for the pyrrole NH binding to various substrates (represented by X) in water and DMSO. The results indicate that the calix[4]pyrrole complexes with $O_2^{\bullet-}$ and $HO_2^{\bullet}$ were the most favorable by 5.5−10.1 kcal/mol and have relatively shorter NH···X bond distances compared to other nonradical substrates (with the exception of the calix[4]pyrrole···Br^- complex). By virtue of symmetry, $O_2^{\bullet-}$ alone gives equivalent charge and spin density distributions between the two oxygen atoms. However, the calix[4]pyrrole···$O_2^{\bullet-}$ complex gave charge distributions of −0.52 and −0.29 e for the internal and terminal oxygens, respectively, and the spin densities were calculated to be 34% (internal O) and 65% (terminal O). As shown in Figure 2, the calix[4]pyrrole···$O_2^{\bullet-}$ complex is characterized by the presence of strong H-bonding (1.84−1.86 Å) between the pyrrole NH and superoxide O. The electronic parameters of $O_2^{\bullet-}$ upon complexation with calix[4]pyrrole are intermediate between the electronic properties of the free $O_2^{\bullet-}$ (−0.5 e and 50% for the charge and spin densities, respectively) and $HO_2^{\bullet}$ (−0.20 e and 70% for the terminal O and −0.36 e and 30% for the internal O). These differences in the electron distributions between $O_2^{\bullet-}$ and $HO_2^{\bullet}$ ($pK_a = 4.8$)[50] translate to higher reactivity of the latter compared to the former with rate constants of $O_2^{\bullet-}/HO_2^{\bullet}$ addition to DMPO of 2.0, 27.0, and $\sim 10^3$ M^{-1} s^{-1} at pH 7.0, 6.2, and 5.0, respectively,[25,51]

(37) Hardy, M.; Bardelang, D.; Karoui, H.; Rockenbauer, A.; Finet, J.-P.; Jicsinszky, L.; Rosas, R.; Ouari, O.; Tordo, P. *Chem.—Eur. J.* **2009**, *15*, 11114–11118.
(38) Allen, W. E.; Gale, P. A.; Brown, C. T.; Lynch, V. M.; Sessler, J. L. *J. Am. Chem. Soc.* **1996**, *118*, 12471–12472. Gale, P. A.; Anzenbacher, P., Jr.; Sessler, J. L. *Coord. Chem. Rev.* **2001**, *222*, 57–102. Gale, P. A.; Sessler, J. L.; Kral, V.; Lynch, V. *J. Am. Chem. Soc.* **1996**, *118*, 5140–5141.
(39) Gale, P. A.; Sessler, J. L.; Kral, V. *Chem. Commun.* **1998**, 1–8.
(40) Aydogan, A.; Sessler, J. L.; Akar, A.; Lynch, V. *Supramol. Chem.* **2008**, *20*, 11–21.
(41) Anzenbacher, P., Jr.; Try, A. C.; Miyaji, H.; Jursikova, K.; Lynch, V. M.; Marquez, M.; Sessler, J. L. *J. Am. Chem. Soc.* **2000**, *122*, 10268–10272.
(42) Anzenbacher, P., Jr.; Jursikova, K.; Shriver, J. A.; Miyaji, H.; Lynch, V. M.; Sessler, J. L.; Gale, P. A. *J. Org. Chem.* **2000**, *65*, 7641–7645.
(43) Nishiyabu, R.; Anzenbacher, P., Jr. *J. Am. Chem. Soc.* **2005**, *127*, 8270–8271.
(44) Panda, P. K.; Lee, C.-H. *Org. Lett.* **2004**, *6*, 671–674.
(45) Sessler, J. L.; Kral, V.; Shishkanova, T. V.; Gale, P. A. *Proc. Natl. Acad. Sci. U.S.A.* **2002**, *99*, 4848–4853.
(46) Bucher, C.; Zimmerman, R. S.; Lynch, V.; Kral, V.; Sessler, J. L. *J. Am. Chem. Soc.* **2001**, *123*, 2099–2100.
(47) Anzenbacher, P.; Nishiyabu, R.; Palacios, M. A. *Coord. Chem. Rev.* **2006**, *250*, 2929–2938.
(48) Akar, A.; Aydogan, A. *J. Heterocycl. Chem.* **2005**, *42*, 931–934.
(49) Miyaji, H.; Anzenbacher, P., Jr.; Sessler, J. L.; Bleasdale, E. R.; Gale, P. A. *Chem. Commun.* **1999**, 1723–1724. Nielsen, K. A.; Cho, W.-S.; Jeppesen, J. O.; Lynch, V. M.; Becher, J.; Sessler, J. L. *J. Am. Chem. Soc.* **2004**, *126*, 16296–16297.
(50) Behar, D.; Czapski, G.; Rabani, J.; Dorfman, L. M.; Schwarz, H. A. *J. Phys. Chem.* **1970**, *74*, 3209–3213.
(51) Allouch, A.; Lauricella, R. P.; Tuccio, B. N. *Mol. Phys.* **2007**, *105*, 2017–2024.

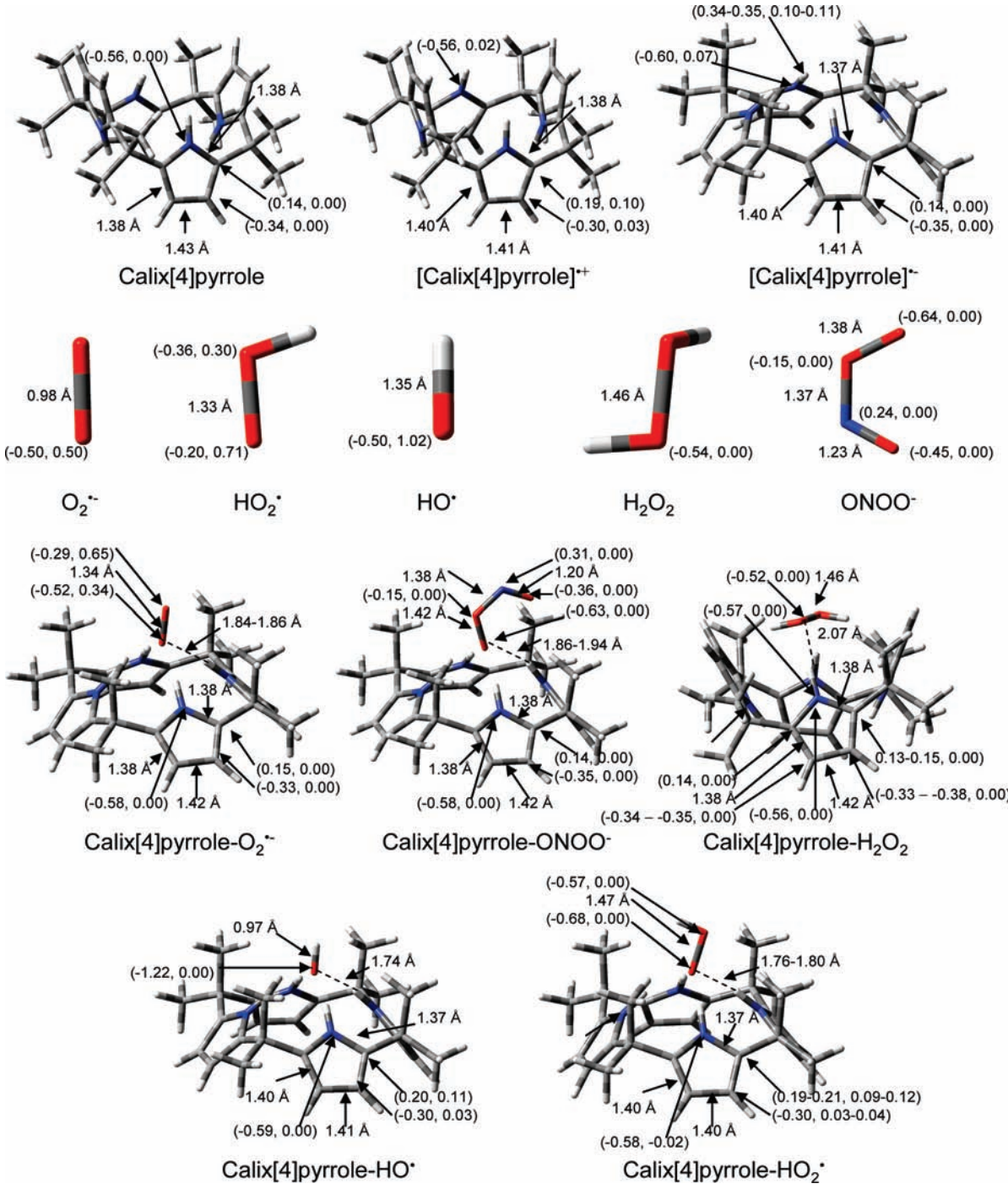

Figure 2. Optimized structures for calix[4]pyrrole complexes including charge (left) and spin (right) densities (in parentheses) and bond lengths (Å) at the PCM(water)/B3LYP/6-31+G(d,p)//B3LYP/6-31G(d) level of theory: first row, octamethylcalix[4]pyrrole and its radical cation and anion; second row, $O_2^{\bullet-}$, $HO_2^{\bullet}$, $HO^{\bullet}$, H_2O_2, and $ONOO^-$; third row, *meso*-octamethylcalix[4]pyrrole complexes with $O_2^{\bullet-}$, $ONOO^-$, and H_2O_2; fourth row, *meso*-octamethylcalix[4]pyrrole complexes with $HO^{\bullet}$ and $HO_2^{\bullet}$.

consistent with reduction potentials of $E^\circ = 0.94$ V for $O_2^{\bullet-}$ and 1.06 V for $HO_2^{\bullet}$.[52] Therefore, this polarization of $O_2^{\bullet-}$ upon complexation with calix[4]pyrrole could enhance $O_2^{\bullet-}$ reactivity with the nitrone similar to our previous observations for the amide-substituted nitrone AMPO[31] and tryosyl radicals in the presence of H-bond donors.[32]

Figure 2 also shows the optimized structures for calix[4]pyrrole and its radical cation and anion forms and complexes with various guest species. The calix[4]pyrrole binding to $HO_2^{\bullet}$ resulted in the disappearance of spin density distributions on the hydroperoxyl O atoms and their redistribution on the methylene carbons of the pyrrole groups. Therefore, electron transfer between $HO_2^{\bullet}$ and calix[4]pyrrole may occur. The calix[4]pyrrole$\cdots HO_2^{\bullet}$ gave charge densities of -0.68 e (terminal O) and -0.57 e (internal O) with an O$-$O bond length of 1.47 Å. These electronic properties are intermediate between those observed for HO_2^- and $HO_2^{\bullet}$ since examination of the charge densities of HO_2^- showed -0.83 e (terminal O) and

(52) McCormick, M. L.; Gaut, J. P.; Lin, T.-S.; Britigan, B. E.; Buettner, G. R.; Heinecke, J. W. *J. Biol. Chem.* **1998**, *273*, 32030–32037.

−0.68 e (internal O) with an O−O bond length of 1.53 Å, while the O−O bond length for $HO_2^{\bullet}$ is 1.33 Å with charges of −0.20 e (terminal O) and −0.36 e (internal O). For comparison, the electronic properties of [calix[4]pyrrole]$^{\bullet+}$ and [calix[4]pyrrole]$^{\bullet-}$ were also investigated. The results indicate that the charges are slightly more positive on α-pyrrolic carbons and less negative on *β*-pyrrolic carbons and there is a higher spin density distribution on all the pyrrole carbon and nitrogen atoms in [calix[4]pyrrole]$^{\bullet+}$ compared to calix[4]pyrrole, while in [calix[4]pyrrole]$^{\bullet-}$, the pyrrole N is more negative and the spin densities are more localized on the pyrrole N and the NH protons. The electronic property of calix[4]pyrrole in the optimized calix[4]pyrrole···$HO_2^{\bullet}$ complex is close to that observed for [calix[4]pyrrole]$^{\bullet+}$, further supporting the oxidation of calix[4]pyrrole by $HO_2^{\bullet}$ to form HO_2^- and [calix[4]pyrrole]$^{\bullet+}$.

The binding energies of calix[4]pyrrole with other biologically relevant reactive species such as peroxynitrite ($ONOO^-$), hydroxyl radical ($HO^{\bullet}$), and hydrogen peroxide (H_2O_2) were also calculated. As shown in Table 1, complex formation of $HO^{\bullet}$ is the most exoergic ($\Delta G_{298K,aq} = -21.6$ kcal/mol), followed by those of $ONOO^-$ and H_2O_2 with $\Delta G_{298K,aq}$ values of 12.3 and 15.9 kcal/mol, respectively. Similar to that observed for the redox reaction between $HO_2^{\bullet}$ and calix[4]pyrrole, $HO^{\bullet}$ binding with calix[4]pyrrole resulted in the formation of HO^- and [calix[4]pyrrole]$^{\bullet+}$ as evidenced by the electronic properties predicted for the optimized calix[4]pyrrole···$HO^{\bullet}$. The binding of $ONOO^-$ and H_2O_2 with calix[4]pyrrole did not result in redox reaction, and their energetics are similar to those expected for the other anionic and neutral substrates. The difference in the exoergicity of calix[4]pyrrole complex formation with $HO^{\bullet}$ and $HO_2^{\bullet}$ is due to their respective reduction potentials of 2.31 V and 1.06 V, respectively.[53] The electrochemical properties of *meso*-octamethylcalix[4]pyrrole have been previously[54] studied using cyclic voltammetry in CH_2Cl_2 and benzonitrile and gave reduction potentials of 0.92 and 0.82 V, respectively, centered at the pyrrole rings. These higher reduction potentials for $HO^{\bullet}$ and $HO_2^{\bullet}$ compared to calix[4]pyrrole support the tendency of calix[4]pyrrole to be oxidized in solution by $HO^{\bullet}$ and $HO_2^{\bullet}$ but due perhaps to the similarity in the reduction potentials of $O_2^{\bullet-}$ and calix[4]pyrrole (i.e., $E^{\circ} = 0.94$ V for $O_2^{\bullet-}$).

Single-point calculations with diffuse functions using the B3LYP/6-311+G(d,p) level of theory were performed to account for the negative charges of some guest ions, and the results indicate no significant difference in the thermochemistry compared to the B3LYP/6-31+G(d,p) level of theory. However, a significant difference was observed for the Br^- complex formation between the two levels of theory, which could be due to its larger size and its more delocalized charge compared to those of the other anions considered in this study. The effect of a countercation on the thermochemistry of complex formation was also explored. Two positions for the Na^+ were considered as shown in Figure S1 (Supporting Information), that is, one where the Na^+ is adjacent to the $O_2^{\bullet-}$ (top) and the other where the Na^+ is below the $O_2^{\bullet-}$ (bottom). The thermodynamics of complex formation for calix[4]pyrrole···$O_2^{\bullet-}$ + Na^+ gave significantly higher endoergic energies compared to the formation of calix[4]pyrrole···$O_2^{\bullet-}$ in which the top and bottom positions for the Na^+ gave $\Delta G_{298K,aq}$ values of 18.2 and 29.7 kcal/mol, respectively, compared to 9.2 kcal/mol in the absence of Na^+. This indicates that formation of the calix[4]-pyrrole···$O_2^{\bullet-}$ + Na^+ complex is not favorable, although Gale and co-workers[55] have determined that, in the solid state, the anion complexes are in close proximity to their countercation. Moreover, inclusion of the countercation leads to a more accurate modeling of NMR spectroscopic data from DFT calculations.[56]

In this work, although the effect of a countercation was not extensively studied for all the complexes, the small difference in the association energy of Na^+ ($\Delta G_{298K,aq} = 3.5$ kcal/mol) with $O_2^{\bullet-}$ compared to calix[4]pyrrole (9.2 kcal/mol) indicates that electrostatic interaction can compete with H-bonding interaction. Also, complexation of $O_2^{\bullet-}$ to Na^+ only resulted in a small perturbation of the electron distribution on the two oxygen atoms with charge distributions of −0.56 and −0.43 e for the internal and terminal oxygens, respectively, and spin densities of 46% (internal O) and 54% (terminal O) (Figure S1, Supporting Information). This small change in electron distribution on $O_2^{\bullet-}$ with Na^+ compared to its complexation with calix[4]pyrrole suggests that the reactivity of $O_2^{\bullet-}$ with nitrone will be more influenced by H-bonding interaction with calix[4]pyrrole than the electrostatic effect with Na^+. Although the thermodynamics of calix[4]pyrrole···$O_2^{\bullet-}$ + Na^+ formation is highly endoergic, the stepwise mechanism for its formation provides better insight into the possible mode of calix[4]pyrrole···$O_2^{\bullet-}$ + Na^+ complex formation in solution. The $\Delta G_{298K,aq}$ for the initial binding of $O_2^{\bullet-}$ to calix[4]pyrrole is 9.2 kcal/mol, which is similar or less endoergic compared to the top or bottom addition of Na^+ to calix[4]pyrrole···$O_2^{\bullet-}$ (see Figure 3). Therefore, the initial binding of $O_2^{\bullet-}$ to calix[4]pyrrole and subsequent addition of the countercation to the calix[4]pyrrole···$O_2^{\bullet-}$ complex is the most plausible mechanism and justifies our consideration of only the anion binding for comparing the various enthalpies and free energies of anion binding to calix[4]pyrrole as shown in Table 1.

2.1.2. Design of the Calix[4]pyrrole−Nitrone Conjugate. Computational studies at the PCM(water)/B3LYP/6-31+G(d,p)//B3LYP/6-31G(d) level of theory were also performed to explore the optimal design that incorporates both the calix[4]pyrrole and nitrone in one molecule. Figure 4 shows three possible spin trap designs where a nitrone and calix[4]pyrrole are coupled via an ester linkage (CalixMPO), two methyl groups were substituted for a pyrroline ring to form a spiro compound (**8**), and one of the pyrrole rings was substituted with a nitrone pyrroline ring (**9**). (The ester linkage was chosen to fully understand the effect of the calix[4]pyrrole moiety on the spin trapping properties of the conjugate since the amide linker group was previously found to exhibit H-bonding properties that can facilitate $O_2^{\bullet-}$ addition to nitrones.) Table 2 and Figure 4 show the thermodynamics of $O_2^{\bullet-}$ addition to CalixMPO, **8**, and **9**, and the CalixMPO−$O_2^{\bullet-}$ adduct gave the lowest free energy of reaction ($\Delta G_{298K,aq}$) of −2.1 kcal/mol compared to the endoergic reaction free energies calculated for compounds **8** and **9** of 26.7 and 31.1 kcal/mol, respectively. Moreover, the addition of $HO_2^{\bullet}$ to CalixMPO is the most favorable with $\Delta G_{298K,aq} = -5.9$ kcal/mol compared to that to **8** and **9** with

(53) Buettner, G. R. *Arch. Biochem. Biophys.* **1993**, *300*, 535–543.
(54) Tabba, H. D.; Cavaleiro, J. A. S.; Jeyakumar, D.; Graca, M.; Neves, P. M. S.; Smith, K. M. *J. Org. Chem.* **1989**, *54*, 1943–1948. Cuesta, L.; Gross, D.; Lynch, V. M.; Ou, Z.; Kajonkijya, W.; Ohkubo, K.; Fukuzumi, S.; Kadish, K. M.; Sessler, J. L. *J. Am. Chem. Soc.* **2007**, *129*, 11696–11697.
(55) Custelcean, R.; Delmau, L. H.; Moyer, B. A.; Sessler, J. L.; Cho, W.-S.; Gross, D.; Bates, G. W.; Brooks, S. J.; Light, M. E.; Gale, P. A. *Angew. Chem., Int. Ed.* **2005**, *44*, 2537–2542.
(56) Nishiyabu, R.; Palacios, M. A.; Dehaen, W.; Anzenbacher, P., Jr. *J. Am. Chem. Soc.* **2006**, *128*, 11496–11504.

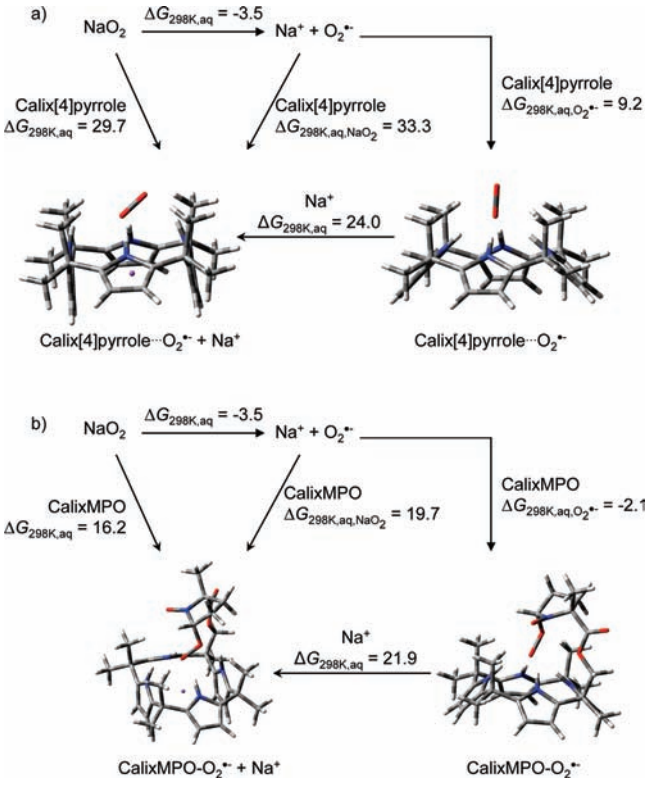

Figure 3. Calculated free energies (kcal/mol) for complex formations of (a) *meso*-octamethylcalix[4]pyrrole and (b) CalixMPO−$O_2^{\bullet-}$ adduct with a sodium countercation (in purple) in the aqueous phase at the PCM/B3LYP/6-31+G(d,p)//B3LYP/6-31G(d) level of theory.

$\Delta G_{298K,aq} = -3.0$ and 11.2 kcal/mol, respectively. The favorable energetics for CalixMPO−$O_2^{\bullet-}$ and CalixMPO−O_2H adduct formations are also reflected in the shorter nitronyl C−$O_2^{\bullet-}$ bond length by 0.06−0.13 Å and slightly shorter nitronyl C−O_2H bond length by 0.01−0.02 Å compared to those of the spin adducts of **8** and **9**. The endoergic free energies of addition of $O_2^{\bullet-}$ and $HO_2^{\bullet}$ to **8** and **9** could be due to steric hindrance, and therefore, the pendant-type CalixMPO is the best candidate for synthesis. Previous studies also showed polymers containing a pendant calixpyrrole subunit exhibiting high affinity toward "hard" potassium salts, thus overcoming the low affinities of calixpyrroles to anions in organic media.[57]

2.1.3. Thermodynamics and Kinetics of $O_2^{\bullet-}$ Addition to CalixMPO. 2.1.3.1. Effect of Calix[4]pyrrole on the Thermodynamics of $O_2^{\bullet-}$ Addition to Nitrones. The mechanism of $O_2^{\bullet-}$ adduct formation at neutral pH proceeds via the rate-limiting nucleophilic addition of $O_2^{\bullet-}$ to the nitrone to form the aminoxyl−$O_2^{\bullet-}$ adduct, which is then followed by protonation to form the aminoxyl−O_2H adduct ($pK_a \approx 15.0$).[58] From here onward, the reference to the formation of $O_2^{\bullet-}$ adducts assumes subsequent protonation in solution to form $HO_2^{\bullet}$ adducts (see eq 1) in a protic medium, and therefore, the $O_2^{\bullet-}$ and $HO_2^{\bullet}$ adducts are used interchangeably.

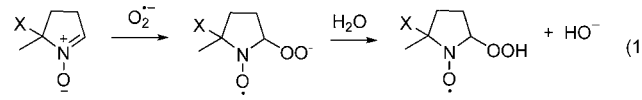

Figure 5 shows the lowest energy conformations for the calix[4]pyrrole···DMPO complex and CalixMPO and their respective $O_2^{\bullet-}$ and $HO_2^{\bullet}$ adducts. A cone-like conformation was exhibited by the unprotonated $O_2^{\bullet-}$ adduct consistent with the conformation of calix[4]pyrroles with anionic guests (e.g., benzoate, Cl^-, Br^-, and CN^-), while 1,3-alternate conformations were found for DMPO−O_2H and CalixMPO−O_2H adducts, which are also consistent with the conformation of calix[4]pyrrole complexes with neutral species such as acetone and MeOH (see the Supporting Information for the optimized structures).[39]

To investigate the effect of the calix[4]pyrrole moiety on the favorability of radical addition to nitrones, the enthalpies and free energies of $O_2^{\bullet-}$ addition to DMPO in the presence of calix[4]pyrrole were calculated and compared to those of CalixMPO (Table 2). Three different scenarios were considered for the formation of calix[4]pyrrole···DMPO−$O_2^{\bullet-}$; that is, mechanism 1 is based on the complex formation from individual calix[4]pyrrole, DMPO, and $O_2^{\bullet}$, mechanism 2 involves complexation of the initially formed DMPO−$O_2^{\bullet-}$ with calix[4]pyrrole, and mechanism 3 includes reaction of the initially formed calix[4]pyrrole···$O_2^{\bullet-}$ with DMPO. The order of increasing favorability for the calix[4]pyrrole···DMPO−$O_2^{\bullet-}$ formation at the PCM(water)/B3LYP/6-31+G(d,p)//B3LYP/6-31G(d) level of theory measured by $\Delta G_{298K,aq}$ (kcal/mol, in parentheses) is mechanism 1 (15.6) < mechanism 3 (6.4) < mechanism 2 (3.0), which indicates that a prior reaction of $O_2^{\bullet-}$ with DMPO or its complexation with calix[4]pyrrole is more favored.

Competition experiments were performed for the spin trapping of $O_2^{\bullet-}$ using DMPO and increasing concentrations of calix[4]pyrrole. In this experiment, solutions containing various molar ratios of DMPO and calix[4]pyrrole were prepared followed by addition of $O_2^{\bullet-}$ to these solutions. As monitored by EPR (see Figure S2a, Supporting Information), there is a significant decrease in the intensity of DMPO−$O_2^{\bullet-}$, suggesting that calix[4]pyrrole can compete with DMPO for binding with $O_2^{\bullet-}$. Furthermore, the decrease in the signal intensity for DMPO−$O_2^{\bullet-}$ observed in the presence of excess calix[4]pyrrole indicates that $O_2^{\bullet-}$ is forming a complex with calix[4]pyrrole, resulting in fast dismutation of $O_2^{\bullet-}$ similar to that observed at

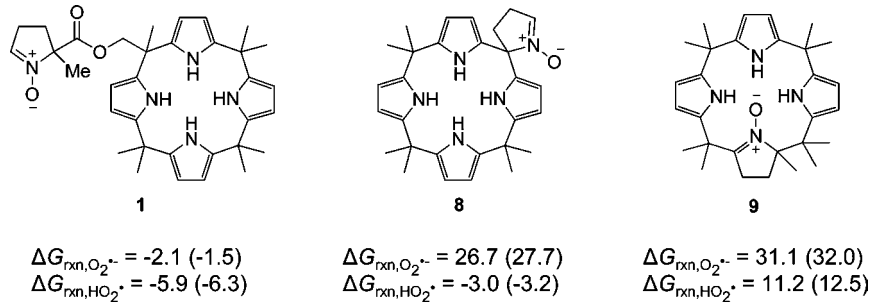

Figure 4. Designs of calix[4]pyrrole-containing nitrone spin traps and their calculated free energies of reaction with $O_2^{\bullet-}$ and $HO_2^{\bullet}$ ($\Delta G_{298K,aq}$, kcal/mol) in the aqueous phase and DMSO (in parentheses).

Table 2. Calculated Enthalpies (ΔH_{298K}) and Free Energies (ΔG_{298K}) (kcal/mol) for $O_2^{\bullet-}$ and $HO_2^{\bullet}$ Spin Adduct Formation with Unconjugated Calix[4]pyrrole···DMPO, CalixMPO, **9**, and **8** in the Aqueous Phase and DMSO (in Parentheses) along with H-Bond Length Ranges (Å) for the Pyrrole NH···O at the PCM/B3LYP/6-31+G(d,p)//B3LYP/6-31G(d) Level of Theory

structure	ΔH_{298K}	ΔG_{298K}	NH···$O_2^{\bullet-}$	NH···O_2H
		Calix[4]pyrrole···DMPO−$O_2^{\bullet-}$		
calix[4]pyrrole + DMPO + $O_2^{\bullet-}$	−9.3 (−11.9)	15.6 (13.0)	1.81−1.86	N/A
calix[4]pyrrole + DMPO−$O_2^{\bullet-}$	−11.4 (−14.9)	3.0 (−0.4)		
calix[4]pyrrole···$O_2^{\bullet-}$ + DMPO	−6.8 (−5.5)	6.4 (7.7)		
		Calix[4]pyrrole···DMPO−O_2H		
calix[4]pyrrole + DMPO + O_2H	−6.6 (−9.8)	15.9 (12.6)	N/A	2.24−2.83
calix[4]pyrrole + DMPO−O_2H	10.3 (6.6)	20.6 (17.0)		
calix[4]pyrrole···O_2H + DMPO	−2.6 (−2.3)	6.6 (7.0)		
CalixMPO−$O_2^{\bullet-}$				
cis-adduct	−16.9 (−16.3)	−2.1 (−1.5)	1.80−1.88	N/A
trans-adduct	−10.0 (−8.8)	5.2 (6.4)	1.76−1.96	
CalixMPO−O_2H				
cis-adduct	−13.9 (−13.6)	−1.9 (−1.6)	N/A	2.31
trans-adduct	−20.6 (−21.0)	−5.9 (−6.3)		2.16
9−$O_2^{\bullet-}$	18.6 (19.5)	31.1 (32.0)	*a*	*a*
9−O_2H	−3.0 (−1.7)	11.2 (12.5)		
8−$O_2^{\bullet-}$	15.3 (16.2)	26.7 (27.7)	*a*	*a*
8−O_2H	−15.2 (−15.4)	−3.0 (−3.2)		

[a] No hydrogen bond observed.

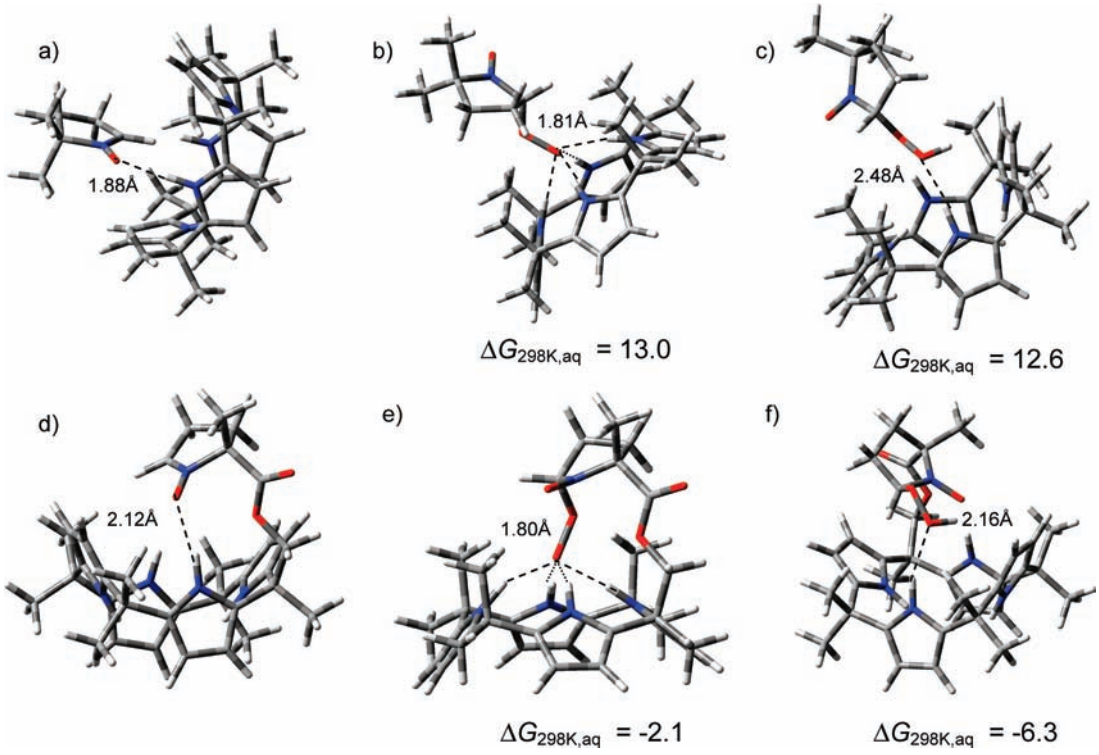

Figure 5. Lowest energy conformations in the aqueous phase of (a) the *meso*-octamethylcalix[4]pyrrole + DMPO complex, (b) the *meso*-octamethylcalix[4]pyrrole + DMPO−$O_2^{\bullet-}$ adduct, (c) the *meso*-octamethylcalix[4]pyrrole + DMPO−O_2H adduct, (d) CalixMPO, (e) the CalixMPO−$O_2^{\bullet-}$ adduct, and (f) the CalixMPO−O_2H adduct with reaction free energies ($\Delta G_{298K,aq}$, kcal/mol) and bond length ranges (Å) at the PCM/B3LYP/6-31+G(d,p)//B3LYP/6-31G(d) level of theory.

slightly acidic pH. Also, in spite of the α-effect caused by calix[4]pyrrole on $O_2^{\bullet-}$, addition of DMPO to calix[4]-pyrrole···$O_2^{\bullet-}$ only results in a significantly lower EPR intensity for the $O_2^{\bullet-}$ adduct formed probably due to the fast dismutation of $O_2^{\bullet-}$ caused by its polarization upon complexation (see Figure S2b, Supporting Information).

The direct addition of $O_2^{\bullet-}$ to CalixMPO gave preference to the formation of the *cis*-adduct ($\Delta G_{298K,aq} = -2.1$ kcal/mol) over the *trans*-adduct ($\Delta G_{298K,aq} = 5.2$ kcal/mol) by ca. 7 kcal/mol. Moreover, the formation of the $O_2^{\bullet-}$ adduct of CalixMPO in the aqueous phase is most preferred compared to DMPO (11.9 kcal/mol), EMPO (9.7 kcal/mol), and AMPO (6.1 kcal/mol) as previously calculated (see Table S1, Supporting Information).[31] These results indicate that the calix[4]pyrrole group and its conjugation to the nitrone play an important role in the favorability of $O_2^{\bullet-}$ addition. The effect of the Na^+ countercation on the thermodynamics of CalixMPO−$O_2^{\bullet-}$ formation was also

(57) Aydogan, A.; Coady, D. J.; Kim, S. K.; Akar, A.; Bielawski, C. W.; Marquez, M.; Sessler, J. L. *Angew. Chem., Int. Ed.* **2008**, *47*, 9648–9652.

(58) Villamena, F. A.; Merle, J. K.; Hadad, C. M.; Zweier, J. L. *J. Phys. Chem. A* **2005**, *109*, 6083–6088.

Table 3. Calculated Relative Enthalpies (ΔH_{298K}) and Free Energies (ΔG_{298K}) (kcal/mol) for $O_2^{\bullet-}$ Addition to Unconjugated and Conjugated Calix[4]pyrrole−Nitrone in the Aqueous Phase and DMSO (in Parentheses) at the PCM/B3LYP/6-31+G(d,p)//B3LYP/6-31G(d) Level of Theory

structure	ΔH_{298K}	ΔG_{298K}	C···$O_2^{\bullet-}$ (Å)	$\langle S^2 \rangle$	imaginary frequency[e]
calix[4]pyrrole···$O_2^{\bullet-}$ + DMPO	0	0	∞	N/A	0
calix[4]pyrrole···$O_2^{\bullet-}$−DMPO	4.9 (6.0)	13.5 (14.6)	3.20	0.76	0
[calix[4]pyrrole···DMPO−$O_2^{\bullet-}$]‡	13.1 (14.3)	25.7 (26.9)	2.03	0.75	432*i*
calix[4]pyrrole···DMPO−$O_2^{\bullet-}$	−6.8 (−5.5)	6.4 (7.7)	1.41	0.75	0
CalixMPO + $O_2^{\bullet-}$ [a]	0	0	∞	N/A	0
CalixMPO···$O_2^{\bullet-}$ [b]	−5.0 (−4.0)	7.1 (8.1)	3.44	0.76	0
[CalixMPO−$O_2^{\bullet-}$]‡ [c]	2.9 (3.6)	17.5 (18.2)	2.00	0.80	422*i*
CalixMPO−$O_2^{\bullet-}$ [d]	−16.9 (−16.3)	−2.1 (−1.5)	1.39	0.75	0

[a] At infinite separation. [b] Complex. [c] Transition state. [d] Product. [e] In units of inverse centimeters.

investigated. Similar to what is observed for the addition of $O_2^{\bullet-}$ to calix[4]pyrrole, the initial addition of $O_2^{\bullet-}$ to CalixMPO is exoergic (−2.1 kcal/mol) compared to the subsequent endoergic addition of Na^+ to CalixMPO−$O_2^{\bullet-}$ of 21.9 kcal/mol (see Figure 3).

Figure S3 (Supporting Information) shows the correlations between the charge densities on the nitronyl C of the various spin traps and the free energies of $O_2^{\bullet-}$ adduct formation at the PCM/B3LYP/6-31+G(d,p) level. The high positive charge density on the nitronyl C of AMPO compared to other nitrones played an important role in the high rate constant observed for the nucleophilic $O_2^{\bullet-}$ addition to AMPO. However, the calculated charge density for the nitronyl C of CalixMPO at the same level of theory is 0.051 e, which is only slightly lower compared to that of AMPO of 0.060 e, indicating that the electrostatic effect is not the major factor for the high reactivity of CalixMPO toward $O_2^{\bullet-}$ and that this could be due mostly to the α-effect caused by the calix[4]pyrrole group on $O_2^{\bullet-}$. Moreover, the complexation of DMPO to calix[4]pyrrole showed an increase in the charge density on the nitronyl C of DMPO from 0.02 to 0.06 e. This effect of the calix[4]pyrrole group on the electrophilicity of the nitronyl C of EMPO will be further discussed in section 2.2.2.

To further show the effect of the calix[4]pyrrole group on the charge density of nitronyl C, the charge densities were compared in the presence and absence of nitrone and calix[4]pyrrole interaction. In the presence of nitrone−NO···HN−calix[4]pyrrole interaction (in which the nitrone group sits on the annulus of the calix[4]pyrrole), the calculated charge density was found to be 0.051 e, while in the absence of this interaction (see Figure S4, Supporting Information), a lower charge density of 0.035 e was observed, which is closer to that observed for EMPO of 0.040 e. This increase in charge density on C-2 of the nitrone is due to the increased contribution of the resonance form **C** during nitrone−NO···HN−calix[4]pyrrole H-bond formation.

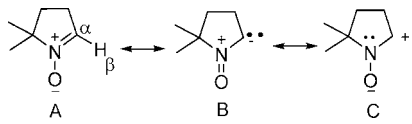

Since CalixMPO has an ester linker group and is not conjugated by an amide bond that would allow facilitation of $O_2^{\bullet-}$ addition to the nitrone through the amide NH, the presence of pyrrole NH in CalixMPO and the proximity of the calix[4]pyrrole ring to the nitrone could play a major role in the facilitation of $O_2^{\bullet-}$ addition to the nitrone group via electrostatics and H-bonding.

2.1.3.2. Effect of Calix[4]pyrrole on the Energy Barrier of $O_2^{\bullet-}$ Addition to Nitrones. The energy barrier for the addition of calix[4]pyrrole···$O_2^{\bullet-}$ to DMPO was calculated to be $\Delta G^{\ddagger}_{298K,aq}$ = 25.7 kcal/mol (Table 3), and this value is similar to that observed for the formation of [DMPO−$O_2^{\bullet-}$]‡ (or close in the case of [EMPO−$O_2^{\bullet-}$]‡ with $\Delta G^{\ddagger}_{298K,aq}$ = 21.1 kcal/mol) as previously calculated (Table S1, Supporting Information).[31] Although polarization of the electronic distribution in $O_2^{\bullet-}$ upon complexation with calix[4]pyrrole has been observed as discussed in section 2.1.1, the energy barrier for the calix[4]pyrrole···$O_2^{\bullet-}$ addition to DMPO was not lowered, indicating that the proximity of the nitrone to the polarized $O_2^{\bullet-}$ is again necessary for facile addition of $O_2^{\bullet-}$ to the nitrone. Table 3 also shows the energy barrier for CalixMPO−$O_2^{\bullet-}$ adduct formation with $\Delta G^{\ddagger}_{298K,aq}$ = 17.5 kcal/mol, which is comparable to that previously[31] calculated for AMPO with $\Delta G^{\ddagger}_{298K,aq}$ = 17.4 kcal/mol. Although the substituent directly attached to CalixMPO is an ester group, the energy barrier observed for CalixMPO is lower compared to that of EMPO but comparable to that of AMPO, which bears an amide substituent. However, examination of the [CalixMPO−$O_2^{\bullet-}$]‡ structure revealed that $O_2^{\bullet-}$ exhibits a strong H-bond interaction with the four pyrrole NH groups prior to the C−O bond formation to form the adduct. This observation is similar to that observed for the [AMPO−$O_2^{\bullet-}$]‡ structure in which the low energy barrier calculated for $O_2^{\bullet-}$ addition to AMPO was previously rationalized to be due to the strong H-bonding interaction between the amide NH and $O_2^{\bullet-}$ in the transition state (TS).

To further confirm the initial mechanism of $O_2^{\bullet-}$ addition to CalixMPO, the most preferred CalixMPO conformation was investigated. The most preferred CalixMPO conformation is when the nitrone moiety is away from the calix[4]pyrrole group, denoted as CalixMPO-180°, as shown in Figure S4 (Supporting Information). The relative free energy of CalixMPO-180° is lower than those of CalixMPO-90° and CalixMPO (**1**) by 0.9 and 3.6 kcal/mol, respectively, which is rationalized to be due to the minimization of steric hindrance. On the other hand, the folded CalixMPO−*cis*-$O_2^{\bullet-}$ adduct ($\Delta G_{298K,rxn}$ = −2.1 kcal/mol) is the most favorable spin adduct conformation, compared to the $O_2^{\bullet-}$ adducts of CalixMPO-180° (15.1 kcal/mol) and CalixMPO-90° (11.7 kcal/mol). Since the $\Delta G_{298K,rxn}$ of $O_2^{\bullet-}$ complexation with calix[4]pyrrole is around 9.2 kcal/mol and the $O_2^{\bullet-}$ addition to the nitrone moiety of CalixMPO-180° to give CalixMPO−*cis*-$O_2^{\bullet-}$ gave $\Delta G_{298K,rxn}$ = 18.3 kcal/mol, it can be expected that the initial addition to the calix[4]pyrrole can occur. These results support the mechanism in which $O_2^{\bullet-}$ adds to the calix[4]pyrrole group of CalixMPO-180° and then the calix[4]pyrrole···$O_2^{\bullet-}$ complex facilitates addition to the nitrone group to give the preferred folded CalixMPO−*cis*-$O_2^{\bullet-}$ adduct as stabilized via intramolecular H-bonding interaction through the pyrrole NH groups.

The "anchoring" of $O_2^{\bullet-}$ to the amide NH results in the polarization of the $O_2^{\bullet-}$ electron distribution known as the

Scheme 1. Synthesis of CalixMPO (**1**) and Structures of Intermediates **2**−**7**

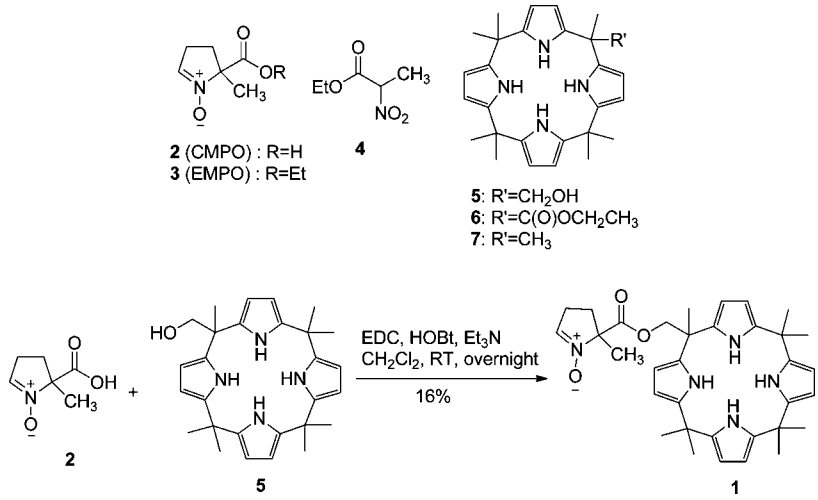

α-effect.[31] Although the energy barriers for the formation of $[CalixMPO-O_2^{\bullet-}]^{\ddagger}$ and $[AMPO-O_2^{\bullet-}]^{\ddagger}$ are almost similar, the calculated $\Delta G_{298K,aq}$ values for the formation of $CalixMPO-O_2^{\bullet-}$ and $AMPO-O_2^{\bullet-}$ are significantly different, in which the former is exoergic (−2.1 kcal/mol) compared to the latter (6.1 kcal/mol), indicating that $O_2^{\bullet-}$ addition to CalixMPO can be both thermodynamically and kinetically favorable compared to that to other nitrones considered in this study. On the basis of the similarity in the $\Delta G^{\ddagger}_{298K,aq}$ for $[CalixMPO-O_2^{\bullet-}]^{\ddagger}$ and $[AMPO-O_2^{\bullet-}]^{\ddagger}$, and the more stable final state for $CalixMPO-O_2^{\bullet-}$ compared to $AMPO-O_2^{\bullet-}$, the potential energy surface for the $CalixMPO-O_2^{\bullet-}$ formation can be visualized to have a reactant-like or early-transition-state surface. This study also further shows the necessity of having the H-bond donor at close proximity to the nitrone moiety, which can obviously be achieved via conjugation, thus allowing a concerted mechanism by which $O_2^{\bullet-}$ can undergo H-bond interaction, resulting in its polarization and eventual facile addition to the nitrone.

2.1.4. Thermodynamics of $HO_2^{\bullet}$ Addition to CalixMPO. Allouch et al.[51] showed that the $O_2^{\bullet-}$ reactivity with nitrones in acidic pH was enhanced due to the formation of $HO_2^{\bullet}$. We have previously proposed that, in acidic pH, the direct addition of $HO_2^{\bullet}$ to the nitrone was the major mechanism for $HO_2^{\bullet}$ adduct formation.[58] The thermodynamics of $HO_2^{\bullet}$ addition to DMPO in the presence of calix[4]pyrrole and to CalixMPO were also investigated. As shown in Table 2, prior complexation of $HO_2^{\bullet}$ to calix[4]pyrrole is the most preferred (6.6 kcal/mol), but unlike for $O_2^{\bullet-}$, the complexation of $DMPO-O_2H$ is the least preferred (20.6 kcal/mol). Nevertheless, $HO_2^{\bullet}$ addition to CalixMPO is exoergic, with the *trans* addition being more favored than *cis* addition with $\Delta G_{298K,aq} = -5.9$ and −1.9 kcal/mol, respectively, contrary to the preferred mode of $O_2^{\bullet-}$ addition (i.e., *cis*), which further supports our hypothesis that prior complexation of $O_2^{\bullet-}$ to the calix[4]pyrrole moiety occurs for the facile $O_2^{\bullet-}$ addition to nitrone. The previously calculated $\Delta G_{298K,aq}$ values (kcal/mol) of $HO_2^{\bullet}$ addition to nitrone at the same level of theory are −0.9 (PBN),[59] −1.6 (AMPO),[60] −4.8 (DEPMPO),[60] −6.2 (EMPO),[60] and −4.6 (DMPO),[60] and these energies are comparable to the formation of the $CalixMPO-O_2H$ adduct with an exoergic $\Delta G_{298K,aq}$ of −5.9 kcal/mol, indicating that the calix[4]pyrrole group has no significant effect on the reactivity of $HO_2^{\bullet}$. This further supports our initial findings that the nature of $HO_2^{\bullet}$ addition to nitrones is mostly electrophilic in nature, contrary to the nucleophilic nature of $O_2^{\bullet-}$ addition to nitrones.[31,60]

2.2. Synthesis and Characterization. 2.2.1. Synthesis of CalixMPO. The synthesis of CalixMPO (**1**) is shown in Scheme 1. The calix[4]pyrrole ethyl ester (**6**) was first synthesized in one step from pyrrole, ethyl pyruvate, and acetone in the presence of methanesulfonic acid in methanol.[40] Subsequently, the ester **6** was reduced by $NaBH_4$ in $EtOH/H_2O$ to the monohydroxycalix[4]pyrrole (**5**) in 75% yield.[61] Finally, the efficient coupling between CMPO (**2**)[62] and the alcohol **5** using EDC, HOBt, and a catalytic amount of Et_3N in CH_2Cl_2 or CH_3CN resulted in the nitrone conjugate of calix[4]pyrrole (**1**) with a yield of 16%, which was well characterized by ^1H, ^{13}C, and $^1H-^1H$ COSY NMR, IR, and HRMS spectroscopies. Attempts to use other polar aprotic solvents (e.g., DMF and DMSO) were unsuccessful. In addition, the yield was not improved by extending the reaction time to 48 h or by heating to 40−45 °C.

2.2.2. NMR Studies. 2.2.2.1. Solvent Dependence of the CalixMPO Conformation. Table S2 (Supporting Information) shows the ^1H chemical shifts for compounds **1**−**7**. The H-2 chemical shift for CalixMPO was found to be 5.42 ppm in $CDCl_3$, which is unusually upfield compared to that for EMPO at 6.87 ppm in $CDCl_3$. The $^1H-^1H$ COSY spectrum shows that H-2 for CalixMPO correlates with two methylene peaks (H-3) at 2.14 and 2.24 ppm and long-range coupling with the methyl H-6 peak at 1.67 ppm (Figure 6), but no correlation between H-2 and the protons from the calix[4]pyrrole ring was observed (see the Supporting Information for the full COSY spectrum). On the other hand, H-2 of CalixMPO in DMSO-d_6 was observed at 6.90 ppm, which is very close to the H-2 chemical shift of EMPO (6.99 ppm) in the same solvent (see the Supporting Information). These results indicate that the H-2 chemical shift of CalixMPO is solvent-dependent, presumably due to the difference in conformation of the calix[4]pyrrole moiety in

(59) Durand, G.; Choteau, F.; Pucci, B.; Villamena, F. A. *J. Phys. Chem. A* **2008**, *112*, 12498–12509.
(60) Villamena, F. A.; Merle, J. K.; Hadad, C. M.; Zweier, J. L. *J. Phys. Chem. A* **2007**, *111*, 9995–10001.
(61) Aydogan, A.; Coady, D. J.; Lynch, V. M.; Akar, A.; Marquez, M.; Bielawski, C. W.; Sessler, J. L. *Chem. Commun.* **2008**, 1455–1457.
(62) Stolze, K.; Rohr-Udilova, N.; Hofinger, A.; Rosenau, T. *Bioorg. Med. Chem.* **2008**, *16*, 8082–8089.

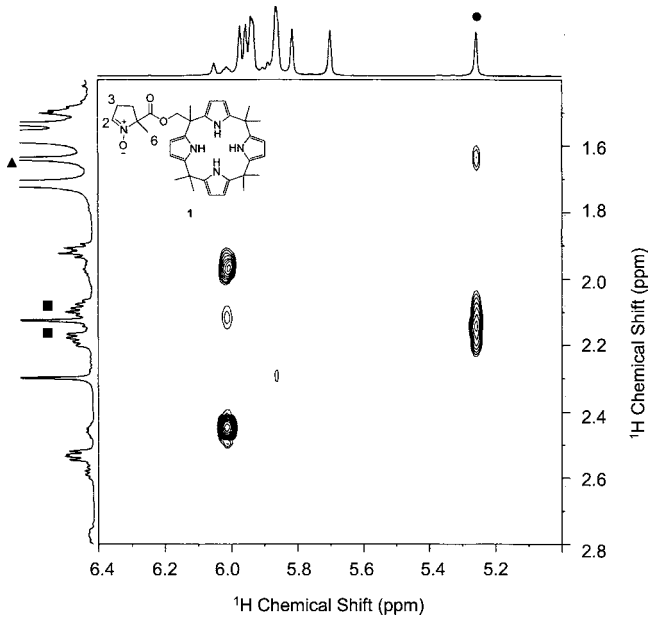

Figure 6. Expanded COSY spectrum of CalixMPO in $CDCl_3$ showing correlation of nitronyl H-2 (●) with H-3 (■) and H-6 (▲).

DMSO and $CHCl_3$, resulting in varying degrees of shielding by the pyrrole groups.

To further investigate the solvent dependence of the chemical shift of H-2 caused by calix[4]pyrrole, the chemical shift of H-2 in DMSO-d_6 was monitored as a function of increasing amounts of $CDCl_3$ (Figure 7). The results show an upfield shift for H-2, suggesting that this proton becomes more shielded in $CDCl_3$. The more downfield chemical shift of H-2 in DMSO-d_6 (6.90 ppm) compared to $CDCl_3$ (5.42 ppm) is due to the less shielding of the nitrone group by the π-systems of the pyrrole rings as they assume a cone-like conformation in DMSO-d_6. The cone-like conformation in DMSO-d_6 is supported by ^{1}H NMR studies as discussed below. However, the 1,3-alternate conformation of the calix[4]pyrrole group in $CDCl_3$ causes higher interaction of the π-systems with the nitrone moiety. This conformation is also supported by the observed ^{1}H NMR shifts in $CDCl_3$, which will be presented in the next section. Computational studies[63] revealed a higher probability of cone conformation in DMSO with a dielectric constant (ε) of 46.7 than in CH_2Cl_2 (ε = 9.1), and since $CHCl_3$ has a dielectric constant of 4.8, which is closer to that of CH_2Cl_2, it can be expected that the cone conformation in $CHCl_3$ is not preferable.

The chemical shifts of pyrrole NH for each of the calix[4]pyrrole-containing compounds (i.e., CalixMPO, **5**, **6**, and **7**) were also investigated (see Figure S5, Supporting Information). In $CDCl_3$, **5** gave two nonequivalent pyrrole NH groups as evidenced by two ^{1}H NMR peaks at 7.05 and 7.54 ppm, and the same ^{1}H NMR profile was observed for **6** with peaks at 7.08 and 7.44 ppm. However, **7** only gave one peak at 6.98 ppm, indicating the presence of four equivalent pyrrole NH groups by virtue of symmetry. However, the four pyrrole NH groups of CalixMPO in $CDCl_3$ are nonequivalent with peaks at 7.36, 7.55, 9.48, and 9.60 ppm, while in DMSO-d_6, the four pyrrole NH groups gave chemical shift values that are close to one another, that is, 9.24,

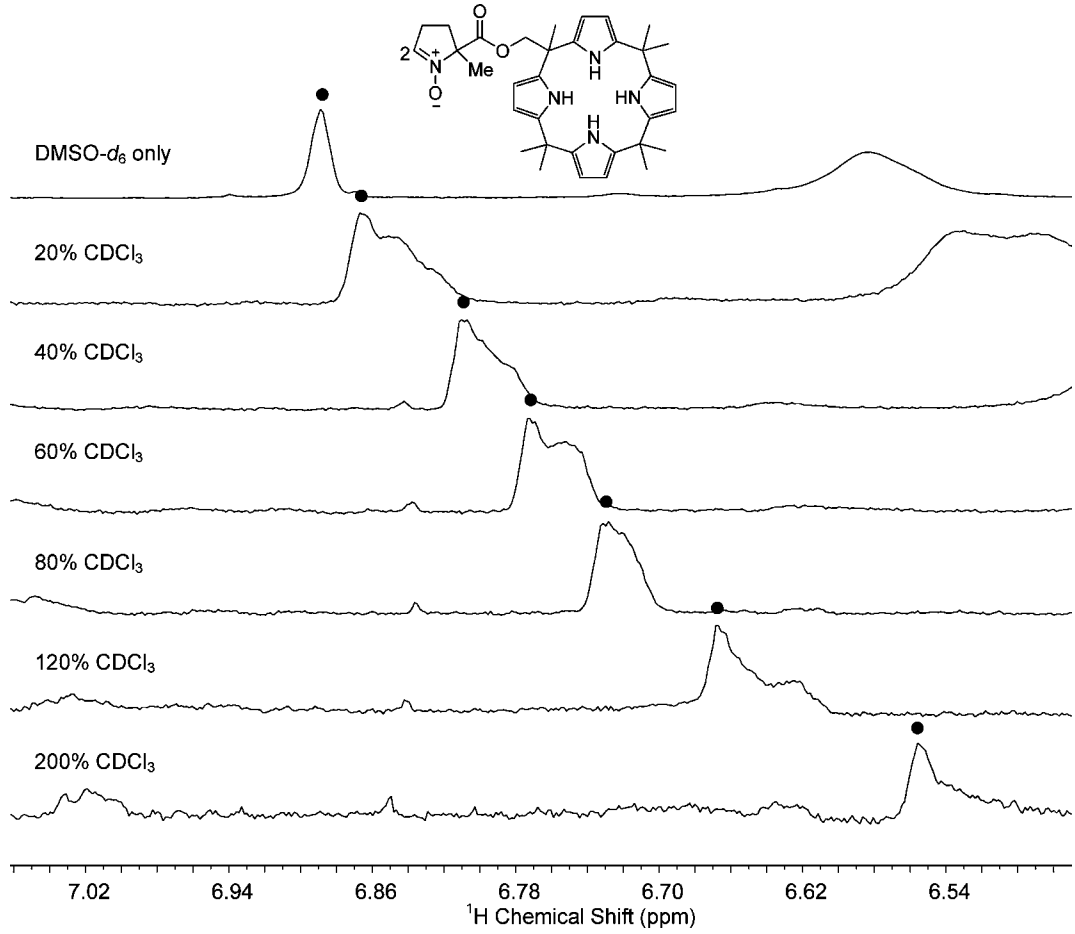

Figure 7. ^{1}H NMR spectra showing the upfield shift of the nitronyl H-2 (●) of CalixMPO as a function of increasing $CDCl_3$ concentrations in DMSO-d_6.

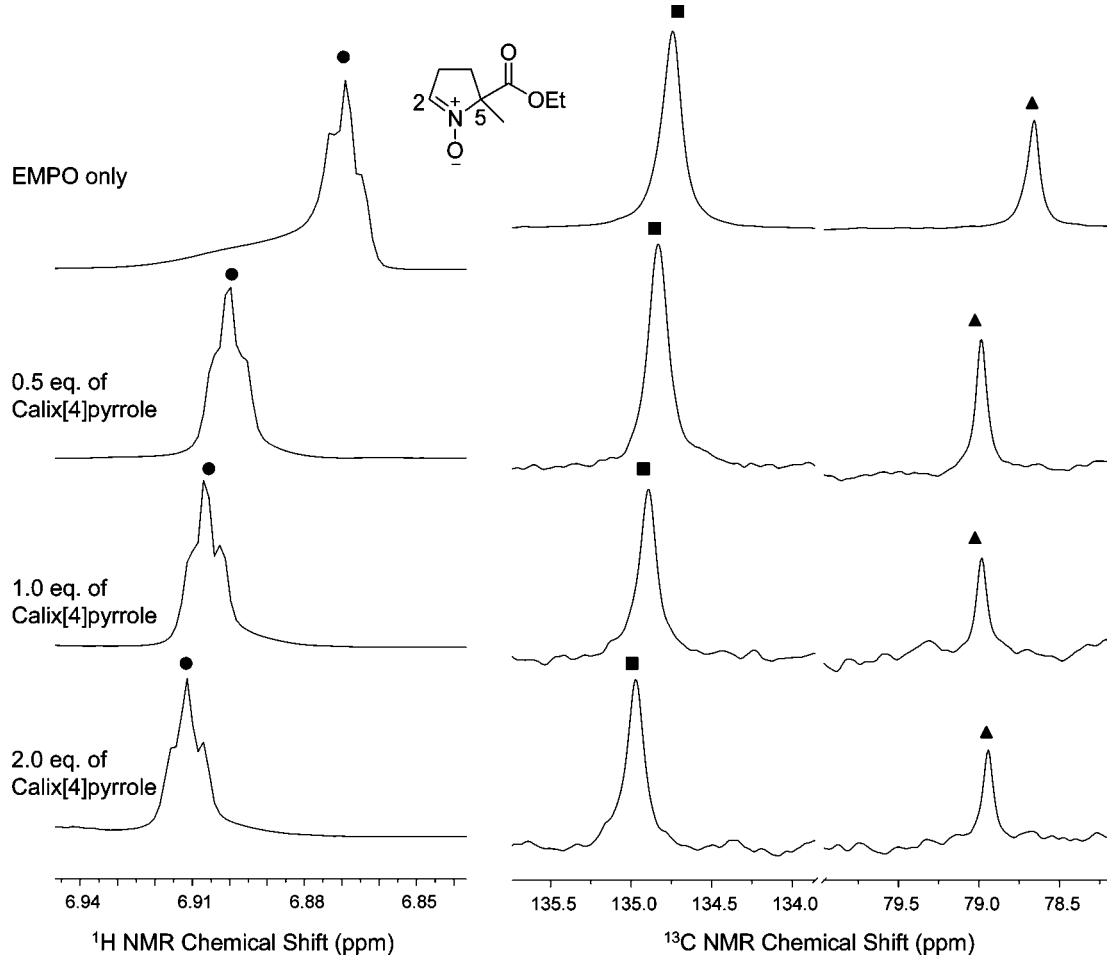

Figure 8. ^{1}H (left) and ^{13}C (right) NMR spectra showing the downfield shift of the nitronyl H-2 (●), C-2 (■), and quaternary carbon (C-5, ▲) of EMPO with increasing number of equivalents of *meso*-octamethylcalix[4]pyrrole in $CDCl_3$.

9.34, 9.46, and 9.51 ppm, due perhaps to the preferred cone-like conformation in this solvent. The difference in ^{1}H NMR spectral profiles for CalixMPO in DMSO-d_6 and in $CDCl_3$ further supports the cone-like and 1,3-alternate conformations in these solvents, respectively.

2.2.2.2. Effect of Calix[4]pyrrole on the C-2 Charge Density. Computational studies show the effect of the calix[4]-pyrrole moiety on the charge density of the nitronyl C. To further confirm these theoretical results, ^{1}H and ^{13}C NMR of EMPO in $CDCl_3$ solutions containing 0.5, 1.0, and 2.0 equiv of *meso*-octamethylcalix[4]pyrrole were obtained. Figure 8 shows that increasing the number of equivalents of calix[4]pyrrole gives a slight downfield shift for H-2, which is characteristic of proton deshielding. Similarly, the ^{13}C NMR chemical shift of C-2 also exhibited a downfield shift (Table S3, Supporting Information) with increasing number of equivalents of calix[4]pyrrole. These NMR results can be rationalized to be due to the intermolecular H-bonding between the pyrrole NH and *N*-oxide O, resulting in a lowered electron density distribution on C-2. A downfield shift in ^{1}H and ^{13}C NMR resonances was also observed for H-2 and C-2 in DMPO as a function of increasing acidity, which was attributed to the protonation of the nitronyl O, resulting in a larger contribution of positive charge on the nitronyl C.[64] This NMR study is consistent with the observations made from the computational studies mentioned above in which the nitrone−NO···HN−calix[4]pyrrole interaction can increase the C-2 charge density.

2.3. EPR Spin Trapping. Spin adducts were generated in mixed solvents due to the poor solubility of CalixMPO in aqueous systems. EPR spectra were generated (Figure 9) from CalixMPO and using various radical-generating systems such as light riboflavin in PBS with 50% acetonitrile, KO_2 in DMSO with 15% PBS, H_2O_2 in pyridine with 10% PBS, and H_2O_2/$FeSO_4$ in PBS with 50% ethanol (see the Experimental Section for details). All the spectra exhibited the dynamic line shape effect as characterized by a broadened line width of the high-field line—characteristic of hindered molecular tumbling due to molecular size and solvent interaction. Parts a−c of Figure 9 gave EPR spectra for the major adduct with a_N and $a_{\beta\text{-H}}$ ranging from 12.39 to 12.95 G and from 10.31 to 11.11 G, respectively. These spectra can be assgined to $HO_2^{\bullet}$ adducts as confirmed by using DEPMPO as a spin trap (see Figure S6, Supporting Information).

Figure 9c shows the EPR spectrum of the $HO_2^{\bullet}$ adduct generated from H_2O_2 in pyridine. The spectrum is relatively clean but with a broader line width and with hyperfine splitting constants (hfsc's) similar to those observed in Figure 9a,b. As we discussed previously,[59] the mechanism for $HO_2^{\bullet}$ adduct formation can occur via nucleophilic addition of HO_2^- to nitrone to yield the hydroxylamine and subsequent oxidation by O_2 to

(63) Bias, J. R.; Lopez-Bes, J. M.; Mirquez, M.; Sessler, J. L.; Javier, F.; Orozco, M. *Chem.—Eur. J.* **2007**, *13*, 1108–1116.
(64) Burgett, R. A.; Bao, X.; Villamena, F. A. *J. Phys. Chem. A* **2008**, *112*, 2447–2455.

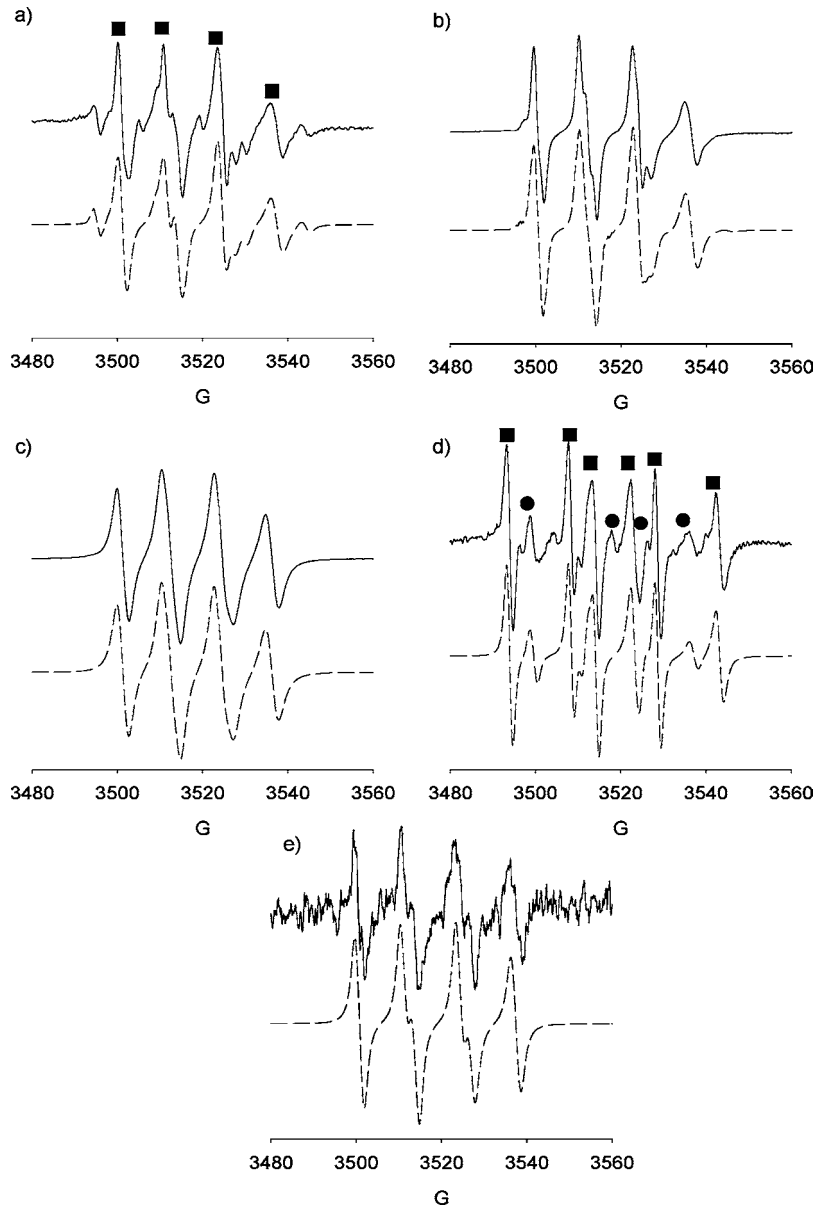

Figure 9. X-band EPR spectra of superoxide adducts of CalixMPO generated from (a) riboflavin/$h\nu$ in 50% CH_3CN in PBS [I, 60% (■), a_N = 12.95 G, a_H = 11.11 G; II, 22%, a_N = 12.58 G, a_H = 8.64 G; alkyl adduct, 18%, a_N = 14.48 G, a_H = 20.70 G], (b) KO_2 in DMSO with 15% PBS (97%, g = 2.0057, a_N = 12.64 G, a_H = 10.61 G; unknown, 3%, g = 2.0054, a_N = 14.40 G, a_H = 19.0 G), and (c) H_2O_2 in pyridine with 10% PBS (100%, g = 2.0058, a_N = 12.39 G, a_H = 10.31 G, $a_{H'}$ = 1.13 G), (d) CH_3•$CHOH$ adduct generated from $H_2O_2/FeSO_4$ in PBS with 50% EtOH [80% (■), g = 2.0054, a_N = 14.51 G, a_H = 20.27 G] and HO• adduct [20% (●), g = 2.0056, a_N = 13.38 G, a_H = 10.80 G], and (e) HO• adduct generated from $H_2O_2/FeSO_4$ in PBS with 50% acetonitrile (g = 2.0056, a_N = 13.02 G, a_H = 10.65 G).

afford the aminoxyl adduct or through direct HO_2• addition to the nitrone, but the latter mechanism is more plausible due to the higher pK_a of the conjugate acid of pyridine (5.2) compared to H_2O_2 (11.2) and the fact that previous chemistry involving H_2O_2/pyridine shows formation of quinones and enones from aromatic systems, further supporting the radical-mediated reaction. Figure 9d shows the EPR spectrum of the CalixMPO radical adducts generated from $H_2O_2/FeSO_4$ in 50% aqueous ethanolic solution. The spectrum is characteristic of a carbon-centered adduct (~80%) originating from α-hydroxyethyl radical (CH_3•$CHOH$) along with a smaller proportion of HO• adduct (~20%). The simulated spectrum for CalixMPO−OH revealed hfsc's of a_N = 13.38 G and a_H = 10.80 G, which are slightly different from the hfsc's observed for the HO_2• adducts, whose observed a_N values are much lower. The alkyl adducts observed in Figure 9a,d gave a_N = 14.48−14.51 G and a_H = 20.27−20.70 G. The HO• adduct of CalixMPO (Figure 9e) was generated in PBS with 50% acetonitrile and gave hfsc's of a_N = 13.02 G and a_H = 10.65 G, with the observed a_N also being higher compared to those observed for HO_2• adducts. By careful simulations, one should be able to distinguish between the CalixMPO−OH and CalixMPO−O_2H adducts.

2.4. Kinetic Studies. 2.4.1. Kinetics of O_2•$^-$ Adduct Formation. 2.4.1.1. UV−Vis Stopped-Flow Kinetics. Figure 10 shows the EPR spectra of the O_2•$^-$ adduct of DMPO and CalixMPO using the same experimental conditions. The intensity of the CalixMPO−O_2H adduct was ca. 18 times higher than that of DMPO−O_2H, suggesting that CalixMPO has a more efficient O_2•$^-$ trapping ability compared to DMPO. To determine the rate constant (k_2) of CalixMPO trapping of O_2•$^-$, a stopped-flow competitive kinetic study was carried out in DMF according to a published procedure[59] in which the growth of the transient

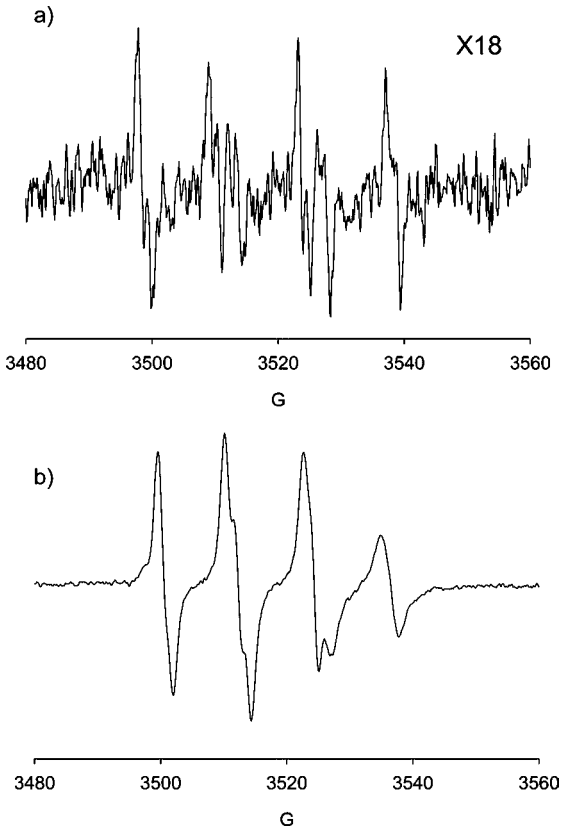

Figure 10. Single-scan EPR spectra of $O_2^{\bullet-}$ adducts of DMPO (15 mM) and CalixMPO (15 mM) generated using KO_2 in DMSO with 15% PBS.

absorption at 575 nm from the reaction between $O_2^{\bullet-}$ and phenol red (PR) was monitored using UV−vis spectroscopy. The relative rate constant was determined using eq 2, where V and υ are the initial rates of the $O_2^{\bullet-}$ reaction with PR in the absence and presence of the nitrone, respectively.

$$\frac{V}{\upsilon} - 1 = \frac{k_{\text{nitrone}}[\text{nitrone}]}{k_{\text{PR}}[\text{PR}]} \qquad (2)$$

Figure 11 shows the plots of $V/\upsilon - 1$ versus [CalixMPO]/[PR] and gives a $k_{\text{CalixMPO}}/k_{\text{PR}}$ of 12.04 ± 1.46, while $k_{\text{DMPO}}/k_{\text{PR}}$ was found to be 0.03 ± 0.00, indicating that CalixMPO traps $O_2^{\bullet-}$ ca. 400 times faster than DMPO in DMF. Using the k_2 determined for DMPO[31] of 1.7 M^{-1} s^{-1}, k_2 for the CalixMPO can be approximated to be ∼680 ± 80 M^{-1} s^{-1}, which is much higher than the previously determined k_2 values in DMF using the same technique, that is, 135 M^{-1} s^{-1} (AMPO),[31] 104 M^{-1} s^{-1} (EMPO),[31] 0.7 M^{-1} s^{-1} (DEPMPO),[31] 0.1−0.8 M^{-1} s^{-1} (PBN),[59] and 221 M^{-1} s^{-1} (C12CDMPO)[34] (see Figure 1 for the structures), indicating that CalixMPO exhibited the highest rate constant for $O_2^{\bullet-}$ trapping in DMF observed thus far for a cyclic nitrone using the same experimental conditions. To investigate the contribution of the calix[4]pyrrole moiety to the observed rate constant for the trapping of $O_2^{\bullet-}$ by CalixMPO, calix[4]pyrrole ethyl ester (**6**) was used for the competitive stopped-flow kinetic studies and shows a relatively high $k_{\text{Calix-OEt}}/k_{\text{PR}}$ ratio of 2.0 ± 0.3 M^{-1} s^{-1}, which indicates that trapping by **6** is ca. 65 times faster than that observed by DMPO. The mechanism for the $O_2^{\bullet-}$ reaction with **6** could be mostly due to dismutation perhaps as catalyzed by the polarization of the spin and charge density distributions as shown by our theoretical studies mentioned above. Due to the proximity of the nitrone

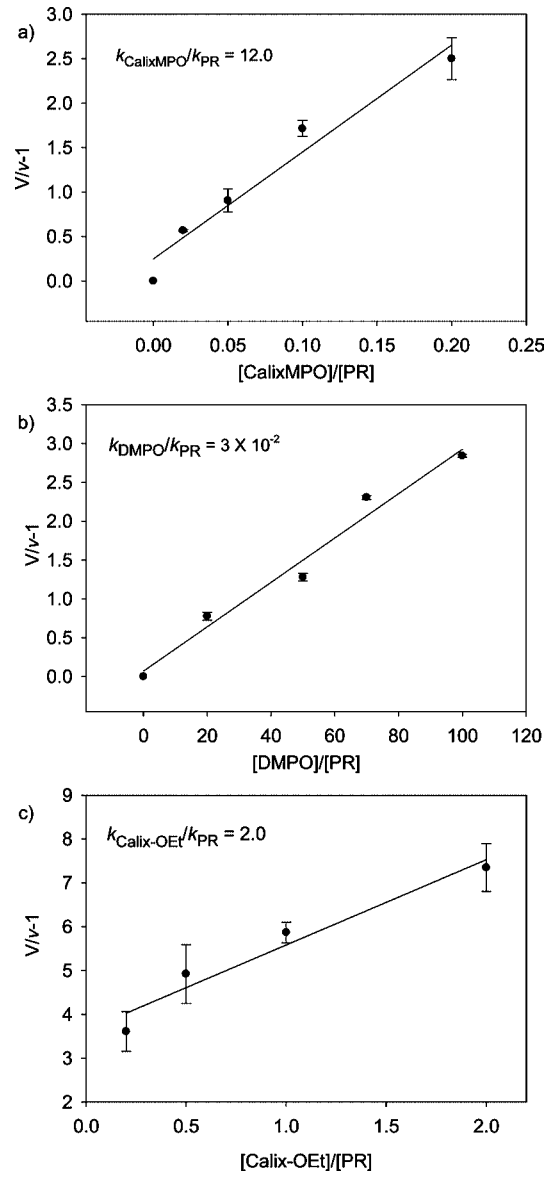

Figure 11. Stopped-flow kinetic plots of the (a) CalixMPO−$O_2^{\bullet-}$ adduct, (b) DMPO−$O_2^{\bullet-}$ adduct, and (c) calix[4]pyrrole ethyl ester−$O_2^{\bullet-}$ complex. Radical was generated using KO_2 in DMF and using PR as the competitor, where V and υ are the initial rates of formation in the absence and presence of various concentrations of the spin trap, respectively.

group to the calix[4]pyrrole moiety, a concerted addition reaction could be a more plausible mechanism in which initial complexation of $O_2^{\bullet-}$ to the calix[4]pyrrole moiety occurs followed by the addition of the electronically polarized $O_2^{\bullet-}$ to the nitrone moiety. This mechanism was similar to the one previously proposed[31] for the amide-substituted nitrones AMPO. Therefore, the presence of the calix[4]pyrrole subunit can greatly improve the $O_2^{\bullet-}$ reactivity with the nitrone.

2.4.1.2. EPR Stopped-Flow Kinetics. The trend in rate constants from the UV−vis stopped flow kinetics was further confirmed by another technique using the EPR stopped-flow method. Due to the limited solubility of CalixMPO in water where the conventional kinetic methodologies for $O_2^{\bullet-}$ radical generation are not possible (e.g., using xanthine−xanthine oxidase or photolysis with riboflavin), a setup was designed such that the reactants could be injected via a syringe directly into the EPR cell to dramatically cut the time from mixing to the initial data acquisition (see the Experimental Section). Only in

Table 4. Calculated Charge Densities (e) of Nitronyl Carbon (C-2), Experimental and Calculated Rate Constants (M^{-1} s^{-1}), and Reaction Free Energies (kcal/mol) for $O_2^{\bullet-}$ Adduct Formation in the Aqueous Phase and DMSO (in Parentheses) at the PCM/B3LYP/6-31+G(d,p)// B3LYP/6-31G(d) Level of Theory

		rate constant			
nitrone	nitronyl C charge density	exptl (k_2)[a]	exptl (k_T)[b]	calcd	$\Delta G_{298K,rxn}$
CalixMPO	0.051 (0.045)	680	8	26.9 (8.5)	−2.1 (−1.5)
AMPO[31]	0.060 (0.059)	130	4	38.7 (19.2)	6.1 (6.4)
EMPO[31]	0.040 (0.038)	105	2	6.8×10^{-2} (2.7×10^{-2})	9.7 (10.3)
DMPO[31]	0.019 (0.018)	2	1	5.9×10^{-5} (1.6×10^{-5})	12.6 (13.8)
DEPMPO[31]	0.043 (0.040)	1	1	1.5×10^{-5} (4.1×10^{-6})	14.7 (15.4)
PBN[59]	0.009 (0.010)	1×10^{-1}	*c*	2.5×10^{-10} (6.3×10^{-11})	18.3 (18.9)

[a] The UV−vis stopped-flow technique was employed with KO_2 and phenol red as competitors in DMF/H_2O (9:1). [b] The EPR stopped-flow technique was employed with KO_2 in DMSO. [c] Not determined.

pure DMSO solutions of KO_2 and nitrones was it found feasible to observe decent signal formation. The experimental conditions do not allow the buildup of signal formation to be followed; thus, a crude estimation by using the maximum adduct concentrations was used and can offer an estimation of the ratios of the trapping rates. For this purpose the lowest nitrone concentration gives the most relevant information; that is, the competition between the dismutation of primary $O_2^{\bullet-}$ formed and the rate of scavenging can determine the maximum concentration. As shown in Figure S7 (Supporting Information), the smallest nitrone concentration is 0.5 mM for CalixMPO, EMPO, and AMPO, where the signal can be observed, while it is 1.0 mM for DEPMPO and DMPO. Moreover, by considering the observed concentrations, we can estimate the ratio of the rate constants k_T. As shown in Table 4, CalixMPO is the fastest spin trap for $O_2^{\bullet-}$ but its rate constant is only 1 order of magnitude faster compared to those of DMPO and DEPMPO. When the decay is very fast, it can also reduce the maximum signal intensity. Therefore, k_T can be underestimated in these cases. For EMPO, AMPO, and CalixMPO, the ratio of the concentrations was 1:2:4, which corresponds to the ratio of the respective rate constants. For DMPO and DEPMPO, the adduct concentrations were the same, and while the necessary nitrone concentration needed to give a detectable result was twice as much as in the case of EMPO, AMPO, and CalixMPO, the respective rate constants for DMPO and DEPMPO can be approximated to be half that in the case of EMPO. It should be noted that the assumption made in this calculation was that the decay rates were all identical. However, since this is obviously not the case, the suggested ratios for the rate constants are rather approximates, but their order can be correct. The trend nevertheless follows that of the UV−vis stopped-flow technique previously employed.

2.4.1.3. Difference in the Magnitudes of the Rate Constant Values between UV−vis and EPR Techniques. The observed trend in rate constants using the UV−vis technique correlates well with the EPR in which the order of decreasing reactivity with $O_2^{\bullet-}$ is as follows: CalixMPO > AMPO > EMPO > DEPMPO ≈ DMPO. However, there is a significant discrepancy in the magnitudes of the rate constants between the two methods, and this can be due to the fact that the EPR technique only monitors the rate of formation of the nitrone−$O_2^{\bullet-}$ adduct, while the UV−vis stopped-flow technique monitors the rate of $O_2^{\bullet-}$ decay that is dependent on the nitrone's concentration. Moreover, since simultaneous spin adduct formation and decay occur during spin trapping, the EPR technique could not account for the $O_2^{\bullet-}$ adducts that decomposed during spin adduct formation, while the UV−vis stopped-flow technique accounts for *all* of the reactions which deplete the concentration of $O_2^{\bullet-}$ and which depend on the nitrone's concentration. Also, solvent effects can significantly affect the rate of adduct formation and adduct stability as discussed. Reaction in pure DMSO using EPR only allows the addition of $O_2^{\bullet-}$ to the nitrone, while the UV−vis technique considers the reaction of the $HO_2^{\bullet}$ and $O_2^{\bullet-}$ species due to the presence of water. It has been shown that $HO_2^{\bullet}$ exhibits higher reactivity with nitrones compared to $O_2^{\bullet-}$ as we explained above.

2.4.2. Correlation of Experimental and Theoretical Rate Constants. The experimental and calculated rate constants as well as the reaction free energies for the $O_2^{\bullet-}$ adduct formation are presented in Table 4 along with the nitronyl C charge densites of their respective nitrones. In general, the qualitative trend in the calculated rate constants at the PCM(water or DMSO)/B3LYP/6-31+G(d,p)//B3LYP/6-31G(d) level of theory follows that of the experimental values for the nitrones with the exception of AMPO and CalixMPO, the trend in their experimental rate constants not correlating well with the calculated values. However, good correlation can be seen with calculated free energies ($\Delta G_{298K,aq}$) and experimental rate constants for $O_2^{\bullet-}$ adduct formation in an aqueous system and in DMSO, with CalixMPO giving the only exoergic $\Delta G_{298K,aq}$ for $O_2^{\bullet-}$ adduct formation compared to other spin traps. This result suggests future consideration of both the $\Delta G_{298K,aq}$ and $\Delta G^{\ddagger}_{rxn}$ in predicting more accurate experimental rate constants.

It is important to note that the C-2 charge densities are higher for CalixMPO and AMPO compared to other nitrones, but AMPO gave a slightly higher charge density (0.060 e) than CalixMPO (0.051 e), indicating that the electrostatic effect on the nucleophilic addition of $O_2^{\bullet-}$ to CalixMPO is not the main factor for the high rate constant experimentally observed for CalixMPO. Moreover, the lower C-2 charge density in CalixMPO compared to AMPO is due to the difference in the nature of the linker group attached to the parent ring. In spite of the same ester group present in both EMPO and CalixMPO, the latter still exhibits a slightly higher C-2 charge density than the former (0.040 e), indicating that the calix[4]pyrrole group affects the charge density on C-2. This effect is further confirmed by the ^{1}H NMR studies previously discussed in section 2.2.2.2 in which free calix[4]pyrrole enhances the positivity of C-2 of EMPO. This through-space mechanism rather than through-bond inductive effect in enhancing the C-2 positivity by the calix[4]pyrrole group was also demonstrated computationally in which the C-2 charge density is significantly higher (0.051 e) when the nitrone sits on the annulus of the calix[4]pyrrole group and is H-bonded to it compared to when the nitrone group is not-H-bonded, giving charge densities of only 0.035−0.038 e (see Figure S4, Supporting Information).

2.4.3. Kinetics of $O_2^{\bullet-}$ Adduct Decay. Due to the poor solubility of CalixMPO in water, the decay kinetics was investigated in 85% DMSO−15% PBS by monitoring the decay

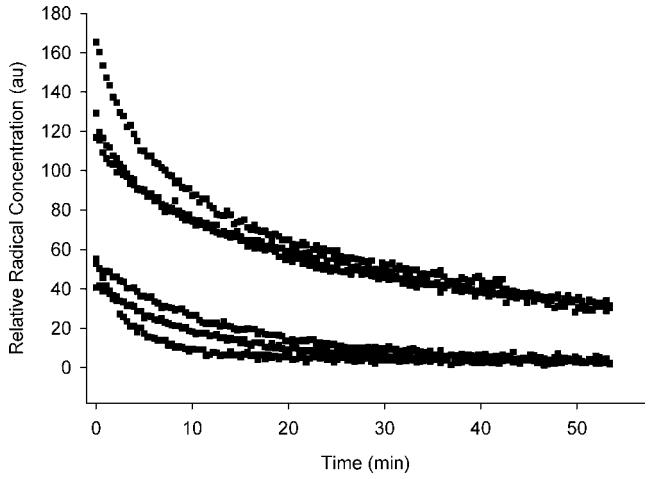

Figure 12. Decay plots for $O_2^{\bullet-}$ adducts generated from CalixMPO (15 mM) and DMPO (15 mM) using KO_2 in DMSO with 15% PBS. The calculated half-lives were ca. 25 and 6 min for CalixMPO−O_2H and DMPO−O_2H, respectively.

of the EPR signal as a function of time and was compared to that of DMPO (Figure 12). As shown in Figure 12, CalixMPO−O_2H exhibited a longer half-life than DMPO, and the half-lives were calculated on the basis of the first-order decay kinetics as 24.9 ± 4.1 and 6.1 ± 1.8 min, respectively. In spite of the potential for DMSO to annihilate the intramolecular H-bond interaction, leading to a short adduct half-life, the longer half-life observed for CalixMPO−O_2H of ∼25 min in DMSO compared to those of CDNMPO−O_2H ($t_{1/2} \approx 6$ min) and C12CDMPO−O_2H ($t_{1/2} \approx 9$ min) could be due to the preference of the calix[4]pyrrole moiety to forcibly assume a cone-type conformation in DMSO, which in turn can stabilize the spin adduct. As shown in Figure 5, the presence of H-bonding of the pyrrole NH with the two hydroperoxyl O atoms is evident and is a potential factor for the adduct stability.

Our previous studies showed that the spirolactonyl nitrone (CPCOMPO) containing a rigid H-bond acceptor exhibited an unstable $O_2^{\bullet-}$ adduct as evidenced by the relatively fast decay ($t_{1/2} = 2.4$ min) of its EPR spectra in aqueous solution.[65] A longer first-order half-life of the $O_2^{\bullet-}$ adduct was achieved from the β-cyclodextrin−nitrone conjugate (CDNMPO), giving a maximum $t_{1/2}$ of 28 min in an aqueous system.[35] This longer half-life for CDNMPO−O_2H was due to the extensive intramolecular H-bonding interaction of the hydroperoxyl moiety with the hydroxyl groups of the cyclodextrin, thus stabilizing the adduct. The effect of H-bonding interaction on the stability of the adduct was further confirmed by measuring the half-life of CDNMPO−O_2H in DMSO as well, and the result shows that $t_{1/2}$ was significantly shortened to ∼6 min due perhaps to the destruction of H-bond interaction in DMSO, indicating that intramolecular H-bonding interaction plays a major role in adduct stability (see Figure 1 for the structures). Aside from the role of intramolecular H-bonding interaction in adduct stability, it is also important to emphasize the better protection of calix[4]pyrrole on the adduct against attack of the primary radical, $O_2^{\bullet-}$, compared to any other trap. We previously[66] showed the redox reaction of $O_2^{\bullet-}$ adducts with $O_2^{\bullet-}$ to form the *N*-olate anion and oxoammonium cation, with the formation of the former being just slightly more favored than that of the latter by ∼0.1 kcal/mol at the PCM/BHandLYP/6-311G(d,p)//B3LYP/6-31G(d) level of theory. The susceptibility of $O_2^{\bullet-}$ adducts to reduction by $O_2^{\bullet-}$ correlates better with their experimental half-lives than their unimolecular decomposition.[67]

The decay kinetics for various nitrones using the EPR stopped-flow technique in pure DMSO was also determined. The decay profile is described by a fast initial decay and then followed by slow decay perhaps due to the fast reaction of the primary radical with the adduct and exhaustion of the radical source, respectively. As shown in Table S4 (Supporting Information), except with CalixMPO, the initial lifetimes of the adducts are very short (i.e., 0.3−1.8 min) in the concentration range of 0.5−15 mM. It appears that these adducts are susceptible to primary radical attack. The CalixMPO adduct seems to be the most protected against the attack of primary radicals with an initial decay time of 5−15 min over a concentration range of 0.5−10 mM. One interesting observation about the $O_2^{\bullet-}$ adduct decay in pure DMSO is the formation of secondary radical adducts (see Figure S8, Supporting Information) from the decomposition of the primary adduct. In 100% DMSO, the primary adduct ($g = 2.0058$, $a_N = 13.2$ G, $a_H = 11.4$ G, $a_{H'} = 1.4$ G) decomposes and new radical species are formed right at the beginning, as opposed to the result in 85% DMSO−15% H_2O, where the primary radical ($g = 2.0057$, $a_N = 12.8$ G, $a_H = 10.7$ G, $a_{H'} = 1.0$ G) is rather stable, with only 4% of other radicals (probably a $HO^{\bullet}$ adduct with $g = 2.0057$, $a_N = 14.4$ G, $a_H = 12.8$ G, and $a_{H'} = 0.6$ G) present.

3. Experimental Section

3.1. Computational Method. All calculations were performed at the Ohio Supercomputer Center. For each structure, an initial conformational search was performed using Spartan 04 at the MMFF level. Density functional theory (DFT)[68] was applied to determine the optimized geometry, vibrational frequency, and single-point energy of all stationary points using Gaussian 03.[69] Single-point energies were obtained at the B3LYP/6-31+G(d,p) and B3LYP/6-311+G(d,p) level on the basis of the optimized geometries. Spin adduct structures were chosen on the basis of the most stable conformer/configurations in aqueous solution and DMSO via the polarizable continuum model (PCM) using single-point energy calculations at the B3LYP/6-31+G(d,p) level.[70] A scaling factor of 0.9806[71] was used for the zero-point vibrational energy (ZPE) correction for the B3LYP geometries. Free energies were obtained from the calculated thermal and entropic corrections at 298 K using the unscaled vibrational frequencies. The charge densities were obtained from a natural population analysis (NPA) approach[72] at the single-point PCM/B3LYP/6-31+G(d,p)//B3LYP/6-31G(d) levels. For the minima, spin contamination for the adduct radicals is negligible, i.e., $0.75 < \langle S^2 \rangle < 0.76$.

3.2. EPR Measurements. EPR measurements were carried out on an EPR spectrometer equipped with a high-sensitivity resonator at room temperature. Unless otherwise indicated, the instrument settings used for general spectral acquisition are microwave power 10 mW, modulation amplitude 1 G, receiver gain 1.0×10^4 or 1.0×10^5, scan time 21.5 s, time constant 42.0 s, and sweep width

(65) Han, Y.; Tuccio, B.; Lauricella, R.; Rockenbauer, A.; Zweier, J. L.; Villamena, F. A. *J. Org. Chem.* **2008**, *73*, 2533–2541.
(66) Villamena, F. A. *J. Phys. Chem. A* **2010**, *114*, 1153–1160.
(67) Villamena, F. A. *J. Phys. Chem. A* **2009**, *113*, 6398–6403.
(68) Labanowski, J. W.; Andzelm, J. *Density Functional Methods in Chemistry*; Springer: New York, 1991.
(69) Frisch, M. J.; et al. *Gaussian 03*; Gaussian, Inc.: Wallingford, CT, 2004.
(70) Villamena, F. A.; Liu, Y.; Zweier, J. L. *J. Phys. Chem. A* **2008**, *112*, 12607–12615.
(71) Scott, A. P.; Radom, L. *J. Phys. Chem.* **1996**, *100*, 16502–16513.
(72) Reed, A. E.; Curtiss, L. A.; Weinhold, F. *Chem. Rev.* **1988**, *88*, 899–926.

120 G. Scans were integrated using the Bruker WINEPR v.2.11b software. All the spin trapping studies were carried out in DMSO or a phosphate buffer (PBS) (10 mM) at pH 7.0 containing 100 μM diethylenetriaminepentaacetic acid (DTPA). Sample cells used were 50 μL glass capillary tubes. The spectrum simulation was carried out by an automatic fitting program.[73]

3.3. Spin Trapping. Superoxide Radical Anion. 3.3.1. KO_2-Generating System. A 100 mM concentration of CalixMPO in DMSO (7.5 μL) was diluted with PBS (7.5 μL) and DMSO (30 μL). Superoxide adduct was generated by adding saturated KO_2 solution in DMSO (5 μL) to the resulting CalixMPO solution (45 μL).

3.3.2. Light-Riboflavin-Generating System. A 20 mM concentration of CalixMPO and 500 μM riboflavin in acetonitrile (20 μL) were diluted with PBS (25 μL) and acetonitrile (5 μL). The resulting solution was bubbled with air for 5 min and then was irradiated using visible light.

3.3.3. H_2O_2/Pyridine-Generating System. A 100 mM concentration of CalixMPO in pyridine (10 μL) was diluted with 35 μL of pyridine. To the resulting CalixMPO pyridine solution was added aqueous 30% H_2O_2 (5 μL).

3.3.4. α-Hydroxylethyl Radical. A 100 mM concentration of CalixMPO in EtOH (7.5 μL) was diluted with EtOH (17.5 μL) and PBS (22 μL). To the resulting CalixMPO aqueous ethanolic solution were added 15% H_2O_2 in PBS (2 μL) and 90 mM $FeSO_4$ in PBS (2 μL).

3.3.5. Hydroxyl Radical. A 10 mM concentration of CalixMPO in acetonitrile (7.5 μL) was diluted with acetonitrile (17.5 μL) and PBS (21 μL). To the resulting CalixMPO solution were added 15% H_2O_2 in PBS (2 μL) and 90 mM $FeSO_4$ in PBS (2 μL).

3.4. Stopped-Flow Kinetics. 3.4.1. UV−Vis Technique. The relative rate constants of $O_2^{\bullet-}$ addition to spin traps were measured using the competitive stopped-flow technique as described in our previous studies.[59] KO_2 was used as the $O_2^{\bullet-}$ source and PR as the competitor. The growth of the transient absorption at 575 nm from the reaction between $O_2^{\bullet-}$ and phenol red was monitored using UV−vis spectroscopy. The plot was linear during the first 5−8 s. The data were fitted to a linear equation ($t = \nu x + c$), where υ is the initial rate of product formation in the presence of various concentrations of spin traps (STs). The resulting initial rates were applied to the following equation: $V/\upsilon - 1 = (k_{ST}[ST])/(k_{PR}[PR])$, where V is the initial rate of formation in the absence of spin traps, k_{ST} and k_{PR} are the rate constants of $O_2^{\bullet-}$ reaction with spin trap and phenol red, respectively, and [ST] and [PR] are the concentrations of spin trap and phenol red (500 μM), respectively. According to the plots of $V/\upsilon - 1$ versus [ST]/[PR], the values of $k_{CalixMPO}/k_{PR}$, $k_{Calix\text{-}OEt}/k_{PR}$, and k_{DMPO}/k_{PR} were determined to be 12.0 ± 1.5, 2.0 ± 0.3, and 0.03 ± 0.00, respectively.

3.4.2. EPR Technique. An AquaX multiple-capillary EPR cell was used for this experiment in which the cell was connected by a 20 gauge regular wall PTFE tube to a mixer that was also connected to two separate 1 mL syringe compartments. The cell was purged with ∼2 mL of DMSO. For all the experiments, the total reaction volume was 1 mL, with one syringe containing 0.5 mL of a solution of the nitrone and the other syringe containing 0.5 mL of a solution composed of 250 μL of KO_2-saturated DMSO diluted with 250 μL of DMSO. The nitrone concentrations (mM) used were 0.02, 0.5, 1.0, 5, and 10. Due to the limited quantity of CalixMPO, only the three lowest concentrations were used for comparison with other nitrones. The two solutions were injected simultaneously after one complete blank scan.

3.5. EPR Decay Kinetics. The KO_2-generating system as the $O_2^{\bullet-}$ source was used. A 100 mM CalixMPO solution in DMSO (7.5 μL) was diluted with PBS (7.5 μL) and DMSO (30 μL). Superoxide adduct was generated by adding saturated KO_2 solution in DMSO (5 μL) to the resulting CalixMPO solution (45 μL). The solution was transferred to a 50 μL capillary tube, and an incremental scan of the EPR spectrum was obtained.

3.6. Kinetic Analysis of EPR Spectra. Analysis of the EPR spectra was carried out by an automatic fitting program.[73] The half-life ($t_{1/2}$) of the adducts was measured by fitting an exponential curve, $\exp[(-\log 2)(t/t_{1/2})]$ to the concentration data from the decay kinetics. For the rate constants of trapping, the EPR measurements only allowed a crude estimation, which offered a trend for the scavenging efficiency of different nitrones. We investigated from a series of nitrone concentrations the lowest concentration where EPR signal can be detected after spin trapping. These concentrations were found to be 0.5 mM for CalixMPO, EMPO, and AMPO and 1.0 mM for DMPO and DEPMPO. At these minimal concentrations, the rate of trapping is slow compared to the dismutation of $O_2^{\bullet-}$, and thus, the buildup rate is proportional to the rate constant of scavenging.

4. Conclusions

Computational studies showed that both $O_2^{\bullet-}$ and $HO_2^{\bullet}$ have higher affinity to calix[4]pyrrole compared to other anions and neutral substrates. Complexation of $HO_2^{\bullet}$ and $HO^{\bullet}$ to calix[4]pyrrole resulted in the formation of HO_2^- and HO^-, respectively, and [calix[4]pyrrole]$^{\bullet+}$. However, complexation of $O_2^{\bullet-}$ with calix[4]pyrrole did not result in redox reaction, but polarization of the electronic properties of $O_2^{\bullet-}$ was evident. The addition of $O_2^{\bullet-}$ to nitrone was thermodynamically and kinetically more favorable when calix[4]pyrrole was conjugated to the nitrone than when there was no conjugation. The thermodynamics of $O_2^{\bullet-}$ complexation to calix[4]pyrrole and its addition to CalixMPO in the presence of Na^+ countercation were also explored, and the results indicate that the H-bond interaction of $O_2^{\bullet-}$ with the calix[4]pyrrole moiety is more preferred than subsequent inclusion of Na^+. Pendant-type conjugation of the nitrone to calix[4]pyrrole was found to be the most efficient design for $O_2^{\bullet-}$ trapping. ^{1}H NMR studies showed that the nitronyl H chemical shift was solvent dependent due to the conformational changes on calix[4]pyrrole, suggesting a shielding effect by the pyrrole moiety. Moreover, H-bond interaction of the calix[4]pyrrole NH groups with the nitronyl oxygen increased the charge density on the nitronyl carbon, the site of radical addition. The $O_2^{\bullet-}$ addition to CalixMPO was exoergic compared to the endoergic reactivity of $O_2^{\bullet-}$ with AMPO, DMPO, EMPO, and DEPMPO, while the energy barrier for $O_2^{\bullet-}$ addition to CalixMPO was comparable to that of AMPO. The $HO_2^{\bullet}$ addition to CalixMPO was comparable to that of EMPO but more exoergic than those of AMPO, DEPMPO, and DMPO, indicating that the nature of $HO_2^{\bullet}$ addition to CalixMPO was electrophilic and that electrostatics and H-bonding played a minor role in the favorability of $HO_2^{\bullet}$ addition to CalixMPO.

Spin trapping using various radical-generating systems yielded $O_2^{\bullet-}$, $CH_3^{\bullet}CHOH$, and $HO^{\bullet}$ adducts and gave robust EPR spectra for $O_2^{\bullet-}$ adduct. Using UV−vis competitive stopped-flow kinetics in DMF/H_2O, the rate constant for the formation of the CalixMPO−$O_2^{\bullet-}$ adduct was approximated to be $k_2 \approx 680$ M^{-1} s^{-1}, which is the highest rate constant observed so far for a nitrone at the experimental conditions used in this work. The high reactivity of $O_2^{\bullet-}$ was rationalized to be due to a synergistic effect from the polarization of $O_2^{\bullet-}$ through H-bonding with calix[4]pyrrole, enhanced positivity of the nitronyl C, and proximity of the nitrone group to the calix[4]pyrrole via conjugation. The half-life of the spin adduct was determined to be $t_{1/2} = 25$ min in DMSO compared to DMPO−$O_2^{\bullet-}$ adduct with $t_{1/2} = 6.1$ min. The high rate constant and long half-life of the CalixMPO−$O_2^{\bullet-}$ formation and decay, respectively, were

(73) Rockenbauer, A.; Korecz, L. *Appl. Magn. Reson.* **1996**, *10*, 29–43.

further independently confirmed by using the EPR stopped-flow technique in pure DMSO and follows the trend observed using the UV−vis competitive stopped-flow method. Since the solubility of CalixMPO in water was limited, the design and synthesis of calix[4]pyrrole that is co-conjugated with solubilizing ligands are now being addressed. This study calls for a future design of spin traps and other probes that incorporates functional anion receptors to be an efficient trap for $O_2^{\bullet-}$. This application of anion receptors can pave the way for a more robust detection of reactive oxygen and nitrogen species and can lead to better understanding of the most important radical-mediated mechanisms in chemical and biological systems.

Acknowledgment. This paper was made possible by Grant RO1 HL81248 from the NIH National Heart, Lung, and Blood Institute. This work was supported in part by an allocation of computing time from the Ohio Supercomputer Center.

Supporting Information Available: Additional figures and tables, synthetic procedures, ^{1}H and ^{13}C NMR spectra of all compounds, COSY, HRMS, and IR spectra of CalixMPO, tables for thermodynamics parameters and Cartesian coordinates, and complete ref 69. This material is available free of charge via the Internet at http://pubs.acs.org.

JA105198C